minerals

MDPI

Article

Geochronology and Geochemistry of Granitic Pegmatites from Tashidaban Li Deposit in the Central Altun Tagh, Northwest China

Kai Kang [1,2,3], Yince Ma [1,2,3], Peng Zhang [4], Hang Li [5,*], Xuehai Wang [1,2,3], Zhaoxia Liao [1,2,3], Lei Niu [6], Jianzhong Chen [4], Xingzhong Liu [4] and Xingwang Xu [1,2,3,*]

1 Key Laboratory of Mineral Resources, Institute of Geology and Geophysics, Chinese Academy of Sciences, Beijing 100029, China; kangkai@mail.iggcas.ac.cn (K.K.)
2 Innovation Academy for Earth Science, Chinese Academy of Sciences, Beijing 100029, China
3 University of Chinese Academy of Sciences, Beijing 100049, China
4 No. 3 Geological Party, Xinjiang Bureau of Geology and Mineral Exploration and Development, Korla 841000, China
5 College of Architecture and Civil Engineering, Sanming University, Sanming 365004, China
6 Exploration and Development Research Institute, Zhongyuan Oilfield Company, SINOPEC, Puyang 457001, China
* Correspondence: lihang16@mails.ucas.ac.cn (H.L.); xuxw@mail.iggcas.ac.cn (X.X.)

Abstract: The Central Altun orogenic system is a result of the amalgamation of multiple micro-continental blocks and island arcs. This complex system originated from subduction–accretion–collision processes in the Proto-Tethys Ocean during the Early Paleozoic. Research has reported the discovery of several Li-Be granitic pegmatite deposits in the Central Altun Block, including the North Tugeman granitic pegmatite Li-Be deposit, Tugeman granitic pegmatite Be deposit, Tashisayi granitic pegmatite Li deposit, South Washixia granitic pegmatite Li deposit, and Tamuqie granitic pegmatite Li deposit. The Tashidaban granitic pegmatite Li deposit has been newly discovered along the northern margin of the Central Altun Block. Field and geochemical studies of the Tashidaban granitic pegmatite Li deposit indicate: (1) Spodumene pegmatites and elbaite pegmatites, as Li-bearing granitic pegmatites that form the Tashidaban granitic pegmatite Li deposit, intrude into the two-mica schist, and marble of the Muzisayi Formation of the Tashidaban Group. (2) Columbite–tantalite group minerals and zircon U-Pb dating results indicate that the mineralization age of Tashidaban Li granitic pegmatites is 450.2 ± 2.4 Ma with a superimposed magmatic event at around 418–422 Ma later. (3) Whole-rock geochemical results indicate that the Kumudaban rock sequence belongs to the S-type high-K to calc-alkaline granites and the Tashidaban Li granitic pegmatites originated from the extreme differentiation by fractional crystallization of the Kumdaban granite pluton.

Keywords: Altun Tagh; rare-metal granitic pegmatite; CGMs and zircon U-Pb dating; magma evolution

check for updates

Citation: Kang, K.; Ma, Y.; Zhang, P.; Li, H.; Wang, X.; Liao, Z.; Niu, L.; Chen, J.; Liu, X.; Xu, X. Geochronology and Geochemistry of Granitic Pegmatites from Tashidaban Li Deposit in the Central Altun Tagh, Northwest China. *Minerals* **2024**, *14*, 542. https://doi.org/10.3390/min14060542

Academic Editor: David Lentz

Received: 7 March 2024
Revised: 16 May 2024
Accepted: 22 May 2024
Published: 24 May 2024

Copyright: © 2024 by the authors. Licensee MDPI, Basel, Switzerland. This article is an open access article distributed under the terms and conditions of the Creative Commons Attribution (CC BY) license (https://creativecommons.org/licenses/by/4.0/).

1. Introduction

Lithium is an essential metal in modern technologies with indispensable applications [1–3], which is widely used in various industries such as glass ceramics, non-ferrous metallurgy, high-energy batteries, nuclear fusion (reactors), and aerospace [1,4]. As an essential source of lithium, petrological studies of the granitic pegmatites is of paramount importance [5–7].

Several large-scale rare-metal mineralization belts have been discovered in China with distributions in the West Kunlun-Songpan-Ganzi orogenic belt, Tianshan orogenic belt, Altai orogenic belt, Qinling-Dabie orogenic belt, Himalaya orogenic belt, Sanjiang orogenic belt, Wuyi-Yunkai orogenic belt, and Jiangnan orogenic belt in recent years [8,9]. Extensive work has been carried out by previous researchers on the formation age of pegmatites [10–17], petrogenesis [18–21], mineralogical characteristics [22–25], magma evolution [26–31], ore-forming

fluids [32–34], and genesis mechanisms of granitic pegmatites [35–40], which significantly enhanced the understanding of rare-metal pegmatites in China.

The Altun Orogenic Belt (AOB) has undergone a complex tectonic evolution from the Archean to Paleoproterozoic with several stages: the formation of the craton and crystalline basement, stable continental margin sedimentation (Middle Paleoproterozoic), continental expansion (Late Neoproterozoic to Early Paleozoic), multiple micro-continents subduction–collision (Paleozoic), and intra-plate evolution (Late Paleozoic to Mesozoic) [41,42]. Tectonic collisions and continental accretion have led to a thickening of the crust in the region, creating conditions that favor the generation of significant magma volumes. Consequently, this has facilitated the formation of highly differentiated pegmatitic magmas [9,37,43]. In recent years, multiple survey results pointed out the significant rare-element mineralization potential in the area. Currently, there are nine rare-metal granitic pegmatite deposits of medium to large scale that have been discovered in the region with mineralization age in 499–445 Ma. These deposits are categorized from southwest to northeast as the Washixia district, the Ayake district, the Kumusayi district, and the Tashidaban district [44–49]. The Washixia district and the Tashidaban district have been preliminarily identified as large to super-large scale. In the northern margin of the AOB, the Tashidaban granitic pegmatite Li deposit is newly discovered in the Tashidaban district with little relevant reports available, currently.

In this study, we firstly presented the geological characteristics of the Tashidaban granitic pegmatite Li deposit and constrained the mineralization age of the Li granitic pegmatites through columbite group minerals (CGMs) and zircon U-Pb dating. The whole-rock geochemical elucidates the petrogenesis of the Kumudaban granitoids and the origin of the Li granitic pegmatites in the Tashidaban granitic pegmatite Li deposit. This study provides a better understanding of the tectonic evolution of the region and facilitates exploration campaigns for Li in the study area.

2. Regional Geological Background

The AOB is a complex tectonic belt subjected to extensive magmatic activity and formed by multiple episodes of subduction–collision in the Early Paleozoic, which traverses the northern margin of the Qinghai-Tibet Plateau in the NE–SW direction. It is sandwiched between the Tarim Block, the Qaidam Block, and the Qilian-Kunlun Orogenic Belt. The tectonic units of the Altun are divided into the Dunhuang block, the North Altun subduction–accretion complex belt (NASB), the Central Altun Block (CAB), the South Altun subduction–collision complex belt, and the Apa-mangya Ophiolitic Mélange Belt from north to south (Figure 1) [50–55].

The Tashidaban granitic pegmatite Li deposit is located on the northern margin of the CAB. The exposed stratigraphy in this area includes the Mesoproterozoic Changcheng System Bashikuergan Group (Ch*B*.), Jixian System Taxidaban Group Muzisayi Formation (Jxm) and Jinyanshan Formation (Jxj), Qingbaikou System Suoerkuli Group (Qb*S*.) and Quaternary sediments. The Bashikuergan Formation consists of a suite of meta-clastic rocks, carbonate, and basic volcanic rocks. Whole-rock Sm-Nd isotopic data from plagioclase amphibolite indicate a Mesoproterozoic age [56]. The Taxidaban Group is a continental clastic–carbonate formation formed at the edge of the marine basin during the tectonic stability period after the consolidation of the transitional basement of the Changcheng System. The U-Pb age of detrital zircons constrains the sedimentary age from the Late Mesoproterozoic to Early Neoproterozoic [57]. The main lithology of the Muzisayi Formation is composed of two-mica schist, quartzite, phyllite, dolomite and garnet-bearing granulite. The main lithology of the Jinyanshan Formation is composed of dolomite, limestone, and marble. The Suoerkuli Group consists of a suite of littoral-to-shallow clastic rocks, carbonate, and volcanic sedimentary rocks. The depositional age indicated by the TIMS U-Pb age of meta-rhyolite (930 Ma) is Neoproterozoic [58].

The regional magmatic activity is characterized by multiple episodes and diverse types of processes exhibiting a northeast to east–northeast trend. The early Paleozoic magmatic

rock types are biotite granite and muscovite granite, with the emplacement age between 522 and 432 Ma [42,44,46–48,59–62].

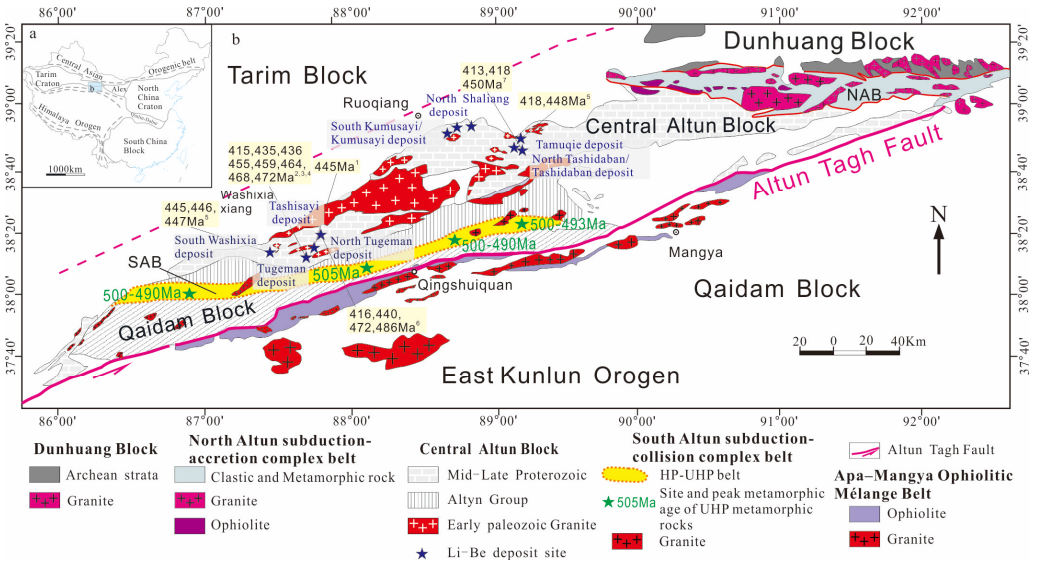


Figure 1. (**a**) Schematic map showing the position of the Altun, NW China, and (**b**) Geological map of Altun, NW China, after [45]. Igneous crystallization and mineralization ages of granitic pegmatite deposits are from: 1—[44]; 2—[46]; 3—[63]; 4—[48]; 5—[64]; 6—[65]; 7—this study.

3. Geology of the Tashidaban Granitic Pegmatite Li Deposit

The Tashidaban Li district includes the Tamuqie granitic pegmatite Li deposit, the North Tashidaban granitic pegmatite Li deposit, and the Tashidaban granitic pegmatite Li deposit. An inferred resource of over 400,000 tons of Li_2O in the district was assessed by the No. 3 Geological Party, Xinjiang Bureau of Geology and Mineral Exploration and Development. The exposed strata in the Tashidaban granitic pegmatite Li deposit include the Bashikuergan Group in the Mesoproterozoic Changcheng System, Jixian System Taxidaban Group in the Muzisayi Formation, and the Jinyanshan Formation. Early Paleozoic Kumudaban pluton is located in the Northwest of the Tamuqie granitic pegmatite Li deposit and intruded the Changcheng System Bashikuergan Group. The pluton consists of fine- to medium-grained biotite monzogranite with the crystallization age of 451~445 Ma [59,62]. The Kumudaban granite facies also includes muscovite granite, albite granite, and tourmaline granite (Figure 2).

The biotite granite (sample 23TD07-5/6) is grey-black and fine- to medium-grained. Quartz (25–30%), plagioclase (30–35%), K-feldspar (20–25%), and biotite (10%) are the primary components with accessory zircon and ilmenite. Biotite occurs as flakes between feldspar and quartz grains and exhibits weak chlorite alteration (Figure 3a). The muscovite granite (sample 21TD22-4/5) is grey-white and medium-grained. Quartz (20–25%), plagioclase (30–35%), K-feldspar (20–25%), and muscovite (10%) are the primary components with accessory garnet (3%), biotite (3%), zircon, and ilmenite. The photomicrograph of Figure 3b depicts muscovite occurring in the form of flakes interspersed between feldspar and quartz grains, exhibiting weak sericite alteration along its edges. The albite granite (sample 23TD06-6/7) is grey-white and fine- to medium-grained. Quartz (30–35%), plagioclase (35–40%), K-feldspar (5–10%), and muscovite (15%) are the primary components with accessory garnet and zircon (Figure 3c). The tourmaline granite (sample 23TD03-1/2) is grey-white and fine- to medium-grained. Quartz (30–35%), plagioclase (30–35%), K-feldspar (5–10%), muscovite (15%), and tourmaline (10%) are the primary components with accessory garnet and zircon. The tourmaline exhibits weak zoning (Figure 3d).

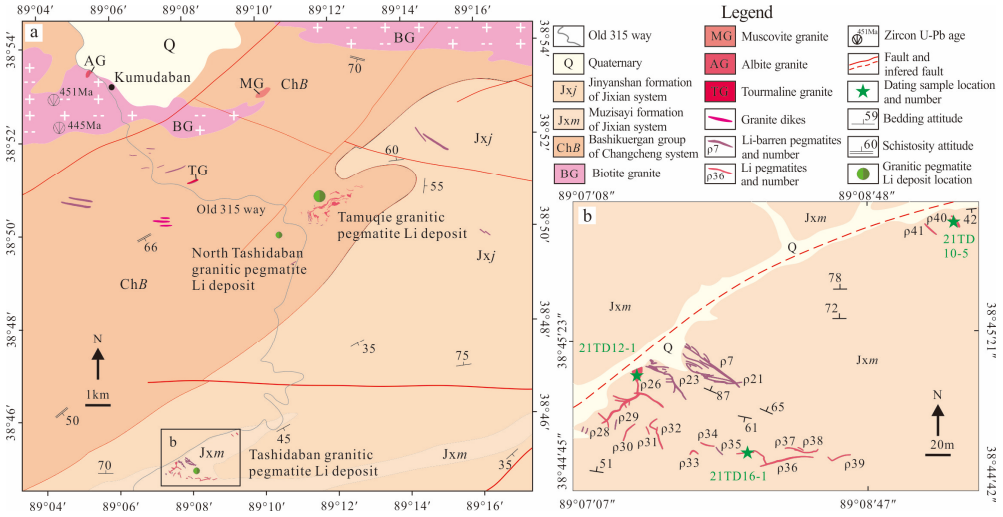


Figure 2. Geological map of (**a**) Kumudaban-Tashidaban area and (**b**) the Tashidaban granitic pegmatite Li deposit.

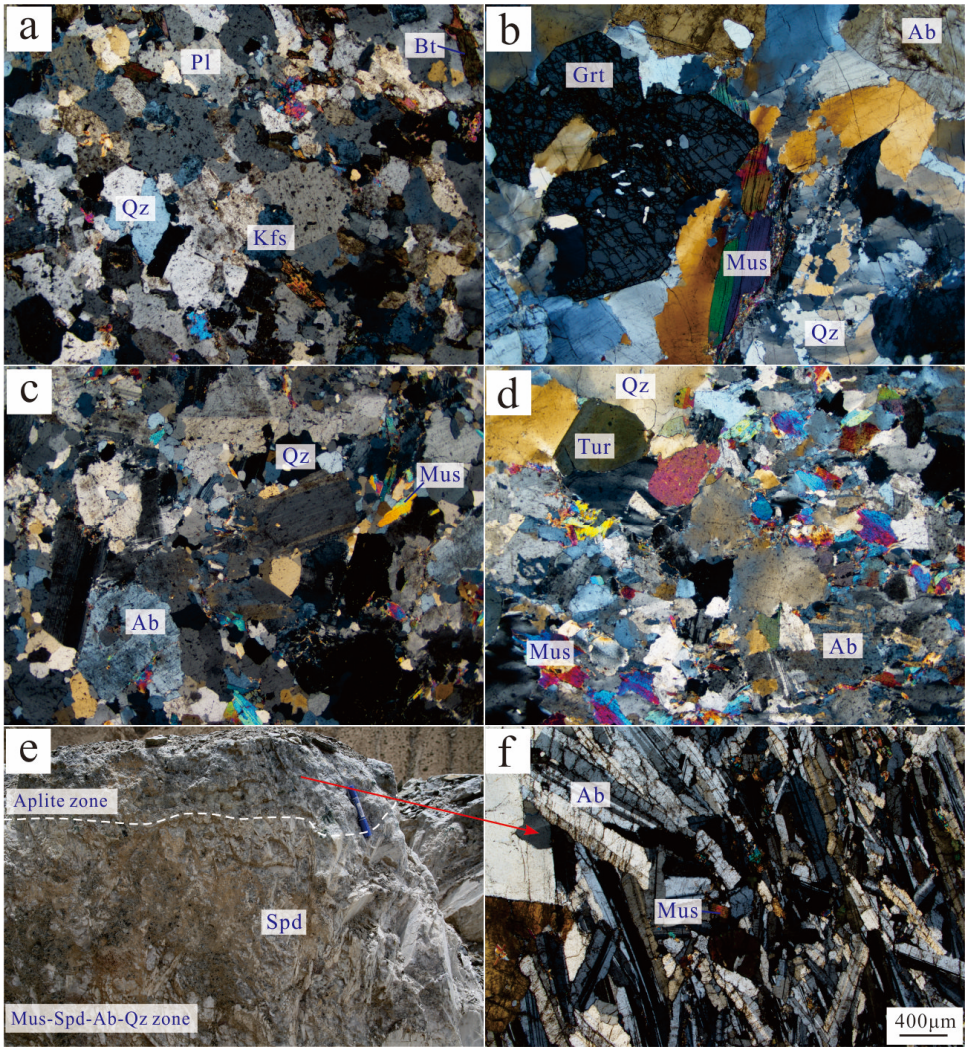


Figure 3. Photographs of the Kumudaban granite facies and pegmatites from the Tamuqie granitic pegmatite Li deposit. (**a**) Photomicrograph of biotite granite from Kumudaban. (**b**) Photomicrograph

of muscovite granite from Kumudaban. (**c**) Photomicrograph of albite granite from Kumudaban. (**d**) Photomicrograph of tourmaline granite from Kumudaban. (**e**) Field photograph of the tρ13 spodumene pegmatite from the Tamuqie granitic pegmatite Li deposit. (**f**) Photomicrograph of the tρ13 spodumene pegmatite from the aplite zone. Abbreviations: Qz: quartz; Pl: plagioclase; Kfs: K-feldspar; Ab: albite; Mus: muscovite; Grt: garnet; Tur: tourmaline; Spd: spodumene.

The Early Paleozoic Suwushijie complex pluton is located in the South of the Tashidaban granitic pegmatite Li deposit and intruded the Jixian System Jinyanshan Formation. The Suwushijie pluton is composed of gabbro–diorite–porphyritic granodiorite fine-grained monzogranite and porphyritic medium-grained monzogranite from early to late [66]. The zircon U-Pb age of monzogranite is 463.6 ± 9.1 Ma and 474.7 ± 5.7 Ma [67]. The muscovite ^{40}Ar-^{39}Ar age is 413.8 ± 7.4 Ma [68], which may represent later hydrothermal events. Several faults cut the metasedimentary rocks in the district with the same direction of the regional deep faults [69].

There are over 50 pegmatite hosted in the Tamuqie granitic pegmatite Li deposit which are located on the northern edge of the district. Among them, more than 40 dykes have a Li_2O grade that meets the standard for industrial mining. The Li-bearing pegmatites represented by spodumene pegmatite contrast with most Li-barren tourmaline-bearing albite pegmatites. The pegmatites concordant with the schist foliation are primarily tabular or lens-shaped intrusions within two-mica schists of the Bashikuergan Group. The main ore-bearing pegmatite dyke, tρ13 spodumene pegmatite, as a whole is approximately 400 m long and is comprised of ten sub-dykes arranged in a left-stepped fashion. CGMs U-Pb dating studies indicated that the tρ13 spodumene pegmatite formed at 448 Ma [64], while ρ8 tourmaline-bearing albite pegmatite formed at 418 Ma [64]. The tρ13 dyke can be classified into the fine-grained albite zone, muscovite–albite–quartz (Mus-Ab-Qz) zone, muscovite–spodumene–albite–quartz (Mus-Spd-Ab-Qz) zone, and Quartz core from outer to inner. The fine-grained albite zone mainly includes muscovite (5~10 vol%), quartz (15~25 vol%), albite (50~60 vol%), and with accessory amounts of apatite, CGMs, and cassiterite (Figure 3e,f).

There are 42 pegmatite dikes hosted in the Tashidaban granitic pegmatite Li deposit, eleven of which have a Li_2O grade that meets the standard for industrial mining (Figure 2). Four types of pegmatite were distinguished in the Tashidaban granitic pegmatite Li deposit, including tourmaline-bearing albite pegmatite, elbaite pegmatite, and spodumene pegmatite. These pegmatites with EW or SE trend intruded into the two-mica schist and marble of the Jixian System Taxidaban Group in the Muzisayi Formation and had a sharp contact with the host rock. For this study, samples were collected from ρ26, ρ36, and ρ40 pegmatite dykes. The pegmatite (ρ40) show a simple internal zoning structure; from the border inward, it can be divided into the elbaite–albite–quartz (Elb-Ab-Qz) zone and aplite zone (Figure 4b). Unlike other zoned pegmatites, aplite zones are not always found in the outer zones of pegmatite [70]. Instead, the aplite zones are dispersed inside pegmatitic dykes, possibly due to multiple episodes of magmatic–hydrothermal developments [71]. The Elb-Ab-Qz zone is characterized by coarse-grained texture (0.3~0.8 cm) and mainly includes quartz (15~20 vol%), albite (30~35 vol%), K-feldspar (5~10 vol%), muscovite (5~10 vol%), elbaite (5~10 vol%), and tourmaline (2~5 vol%), with CGMs and cassiterite as accessory mineral phases (Figures 4e and 5b,c). Coarse-grained quartz with undulose extinction and moderate subgrain orientation displays variable degrees of recrystallization (Figure 5b). The coarse-grained elbaite is replaced by a later fine-grained albite granite (Figure 5c). The aplite zone mainly includes quartz (10~20 vol%), albite (60~70 vol%), apatite (5~10 vol%) and with accessory of CGMs (Figure 5a). The replacement of aplite zone by late-stage fine-grained albite granite can be observed in Figure 5a, and both the aplite zone and albite granite have CGMs intergrown with albite and quartz (Figure 5d,e). The ρ26 tourmaline-bearing albite pegmatite is exposed as a disc-shaped structure on a steep slope with extension in the SE and SW directions with multiple branches. The lithology of the disc-shaped dyke gradually transitions from tourmaline granite to tourmaline-bearing albite pegmatite, a transition marked by a variation in grain size. The tourmaline gran-

ite is grey-white and fine- to medium-grained. Quartz (30–35%), plagioclase (30–35%), K-feldspar (5–10%), muscovite (5%), and tourmaline (10%) are the primary components with accessory zircon and CGMs (Figures 4f and 5f). The ρ36 spodumene pegmatite is 5~8 m wide and 70 m long in an intermittent outcrop. Internal zonation of the aplite zone, muscovite–albite–quartz (Mus-Ab-Qz) zone, spodumene–albite–quartz (Spd-Ab-Qz) zone from border to core characterizes the outcrop (Figure 4c,d). The aplite zone mainly includes quartz (25~35 vol%), albite (30~35 vol%), and muscovite (15~25 vol%) with accessory of CGMs (Figure 5g). The Spd-Ab-Qz zone mainly includes quartz (20~30 vol%), albite (25~30 vol%), spodumene (15~20 vol%), microcline (5~10 vol%), muscovite (5 vol%), and apatite (5~10 vol%) with accessory of CGMs (Figure 5g–i). The coarse-grained quartz intergrown with spodumene has undulose extinction. Recrystallization into granoblastic quartz is observed at the edges of the coarse-grained crystals (Figure 5h,i). Moreover, the replacement of the Spd-Ab-Qz zone by late-stage fine-grained muscovite–albite–granite can be observed (Figure 5i). Distinguished from the aplite zone at the edge of the ρ36 spodumene pegmatite, the content of muscovite in fine-grained muscovite–albite–granite is usually less than 10% by volume.

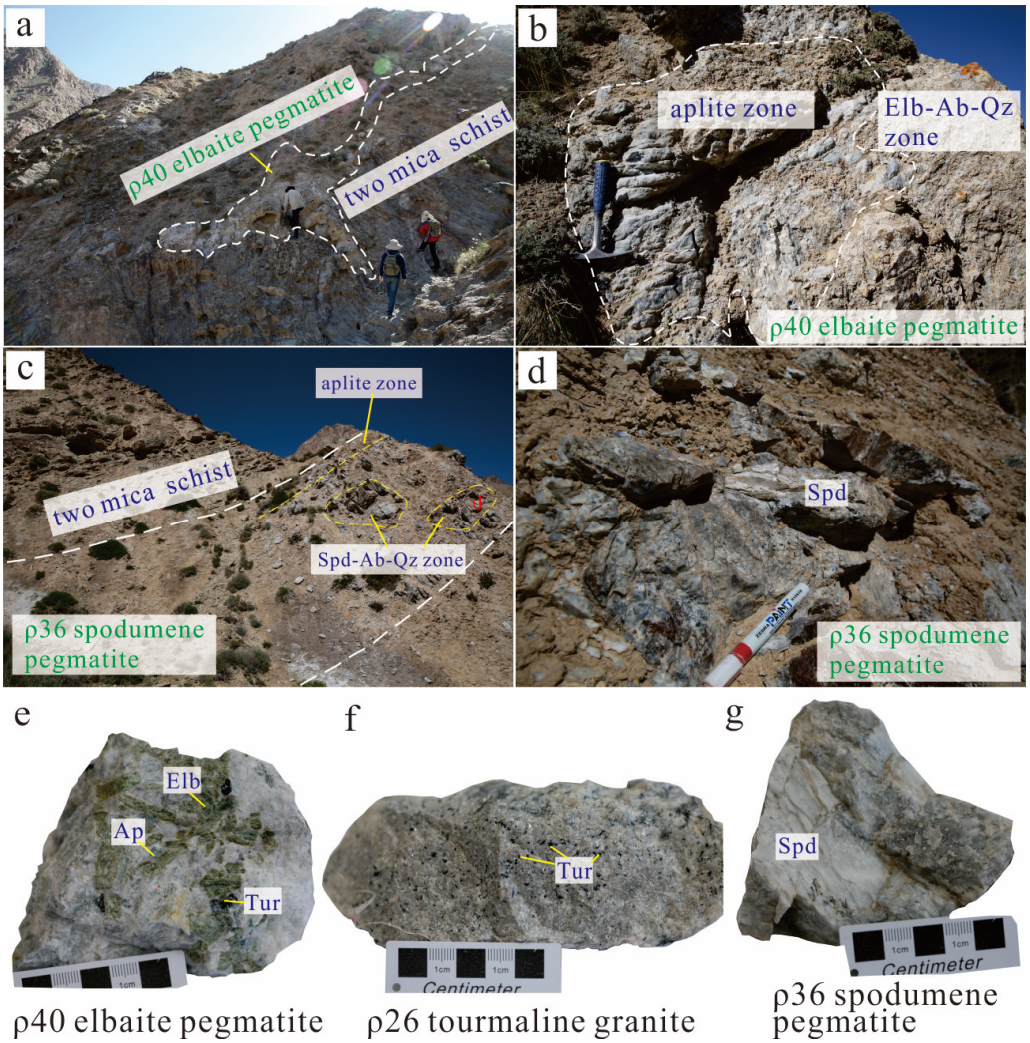


Figure 4. Field photographs of the Tashidaban granitic pegmatite Li deposit and representing hand specimens of the studied pegmatites. (**a**–**d**) Field photographs of the studied pegmatites. (**e**–**g**) Hand specimens of the ρ40 elbaite pegmatite, ρ26 tourmaline granite, and the ρ36 spodumene pegmatite. Abbreviations: Qz: quartz; Ab: albite; Spd: spodumene; Tur: tourmaline; Elb: elbaite.

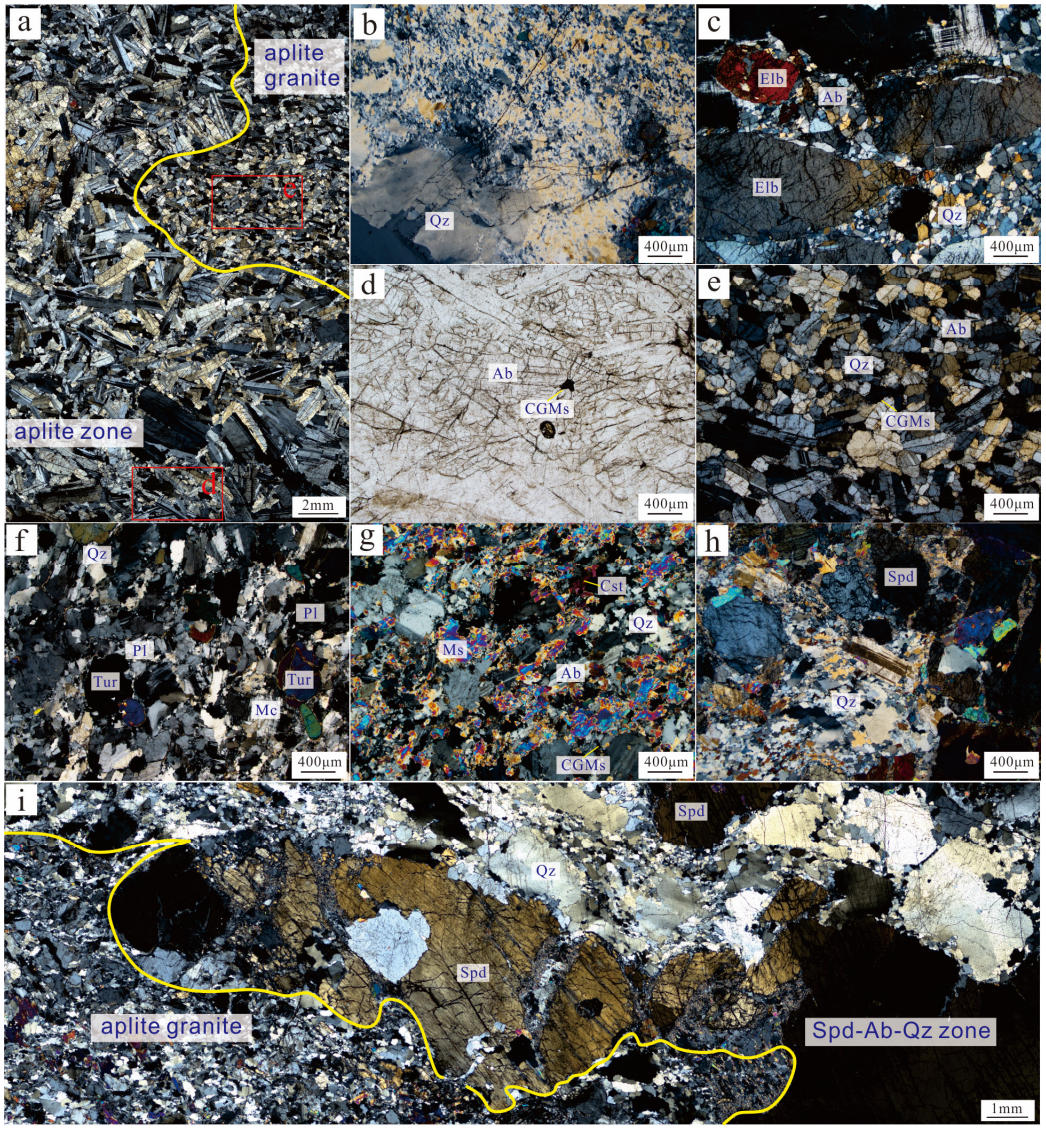


Figure 5. Photographs of the Tashidaban granitic pegmatite Li deposit representing photomicrographs of the studied pegmatites. (**a**–**e**) Photomicrographs of the ρ40 elbaite pegmatite. (**f**) Photomicrograph of the ρ26 tourmaline granite. (**g**) Photomicrograph of the ρ36 spodumene pegmatite from the aplite zone. (**h**,**i**)Photomicrographs of the ρ36 spodumene pegmatite from the Spd-Ab-Qz zone. Abbreviations: Qz: quartz; Ab: albite; Mc: microcline; Ms: muscovite; Spd: spodumene; Tur: tourmaline; Elb: elbaite; CGMs: columbite group minerals; Cst: cassiterite.

4. Sample Selection and Analytical Methods

The samples selection and description are listed in Table 1. The U-Pb dating samples are from the Tashidaban granitic pegmatite Li deposit (Figure 2). Sample 21TD12-1 was collected from the ρ26 tourmaline granite, sample 21TD10-5 was collected from the fine-grained aplite zone of the ρ40 elbaite pegmatite, and sample 21TD16-1 was collected from the fine-grained aplite zone of the ρ36 spodumene pegmatite. The whole-rock geochemical samples are from the vicinity area of the Kumdaban pluton, the Tamuqie granitic pegmatite Li deposit, and the Tashidaban granitic pegmatite Li deposit area.

Table 1. Sample location, rock type, and analytical method for granites and pegmatites.

No.	Location	Sample	Rock Type	Major Trace Elements	Zircon U-Pb Dating	CGM U-Pb Dating
1	Kumudaban	23TD07-5/6	biotite granite	√ (2)		
2		21TD22-4/5	muscovite granite	√ (2)		
3		23TD06-6/7	albite granite	√ (2)		
4		23TD03-1/2	tourmaline granite	√ (2)		
5	Tamuqie Li granitic pegmatite deposit	23TD01-6-1/2	spodumene pegmatite	√(2)		
6	Tashidaban granitic pegmatite Li deposit	21TD10-3/4/5	ρ40 elbaite pegmatite	√ (2)		√
7		21TD16-1/4/5	ρ36 spodumene pegmatite	√ (2)		√
8		21TD12-1/4/5	ρ26 tourmaline granite	√ (2)	√	

The separation of CGMs and zircon was carried out at the Hebei Regional Geological Survey Institute, China. The samples were crushed to particles with sizes of 40 mesh. Based on differences in mineral physical and chemical properties, zircon was separated using gravity separation, while CGMs were separated using magnetic separation. Subsequently, manual handpicking was performed under a binocular microscope to select appropriate mineral grains.

Textural and mineralogical investigations were conducted using a TM4000plus scanning electron microscopy system at the Institute of Geology and Geophysics, Chinese Academy of Sciences (IGGCAS). Back-scattered electron (BSE) images were obtained at an accelerating voltage of 15 kV to illustrate texture features of CGMs minerals. Cathodoluminenscence (CL) imaging was conducted for zircon grain using a JEOL scanning electron microscope at the Institute of Geology and Geophysics, Chinese Academy of Sciences (IGGCAS).

U-Pb dating of columbite was conducted using an ASI RESOlution S-155 193nm ArF Excimer laser coupled to a Thermo Scientific iCAP Qc quadrupole ICP-MS at the State Key Laboratory for Mineral Deposits Research, Nanjing University, China. The diameter of the laser beam was 43 μm, and the laser energy and the repetition rate of laser pulses were set at ~4 mJ/cm^2 and 4 Hz, respectively. The Coltan 139 standard from Madagascar documented U–Pb ages of 505.4 ± 1.0 Ma (BGR, Hannover, Germany; ID–TIMS), 506.6 ± 2.4 Ma (ID–TIMS), and 506.2 ± 5.0 Ma (LA–ICP–MS; Goethe University Frankfurt, Germany) [72,73]. The obtained concordant U-Pb ages of Coltan 139 are 505.5 ± 2.1 Ma (1σ; MSWD = 0.0078) and 505.1 ± 2.3 Ma (1σ; MSWD = 0.055) for samples 21TD10-5 and 21TD16-1, respectively.

U-Pb dating and trace element analysis of zircon was simultaneously conducted by LA-ICP-MS at the Beijing GeoAnalysis CO., LTD, Beijing, China. The NWR193UC model laser ablation system (Elemental Scientific Lasers LLC, Bozeman, MT, USA) was coupled to an Agilent 7900 ICPMS (Agilent, Santa Clara, CA, USA). Detailed tuning parameters can be seen in [74]. The spot size and frequency of the laser were 30 μm and 6 Hz, respectively. Zircon 91,500 (TIMS ^{207}Pb/^{206}Pb age = 1065.4 ± 0.3 Ma, 1 s, n = 11) was used as external standards for U-Pb dating and trace element calibration, respectively. An Excel-based software ICPMSDataCal was used to perform off-line selection and integration of background and analyzed signals, time-drift correction, and quantitative calibration for trace element analysis and U-Pb dating. Concordia diagrams and weighted mean calculations were performed using Isoplot/Ex_ver3 [75].

Whole-rock major and trace elements were determined at ALS Minerals-ALS Chemx, Guangzhou, China. The rock powder was fused with lithium–lithium metraborate flux which also includes an oxidizing agent (Lithium Nitrate), and then poured into a platinum mold. The concentrations of major elements were analyzed by XRF spectrometry. A prepared sample (0.100 g) was added to lithium metaborate/lithium tetraborate flux and fused in a furnace at 1025 °C. The resulting melt was then cooled and dissolved in an acid mixture containing nitric, hydrochloric, and hydrofluoric acids. Trace element

concentrations were analyzed by inductively coupled plasma–mass spectrometry. For lithium analysis, a ~0.4 g sample undergoes an initial digestion process using $HClO_4$, HF, and HNO_3 until complete dryness is achieved. Following this, the residue is further processed through a secondary digestion in concentrated HCl, cooled down, and diluted to the desired volume. Finally, the samples are examined for lithium content using ICPAES spectroscopy.

5. Results

5.1. CL Features and U-Pb Dating Results

The CGM grains in the Tashidaban granitic pegmatite Li deposit from ρ40 elbaite pegmatite are mainly black and subhedral (Figures 5d,e and 6a). Seven analyzed points (Sample number 21TD10-5) varying from 452 to approximately 448 Ma with a weighted mean $^{206}Pb/^{238}U$ age of 450.2 ± 2.4 Ma (1σ; MSWD = 0.37) are shown. Thirteen measured points have a weighted mean $^{206}Pb/^{238}U$ age of 413.0 ± 3.6 Ma (1σ; MSWD = 0.21), varying from 417 to 407 Ma (Figure 7a,b; Table 2).

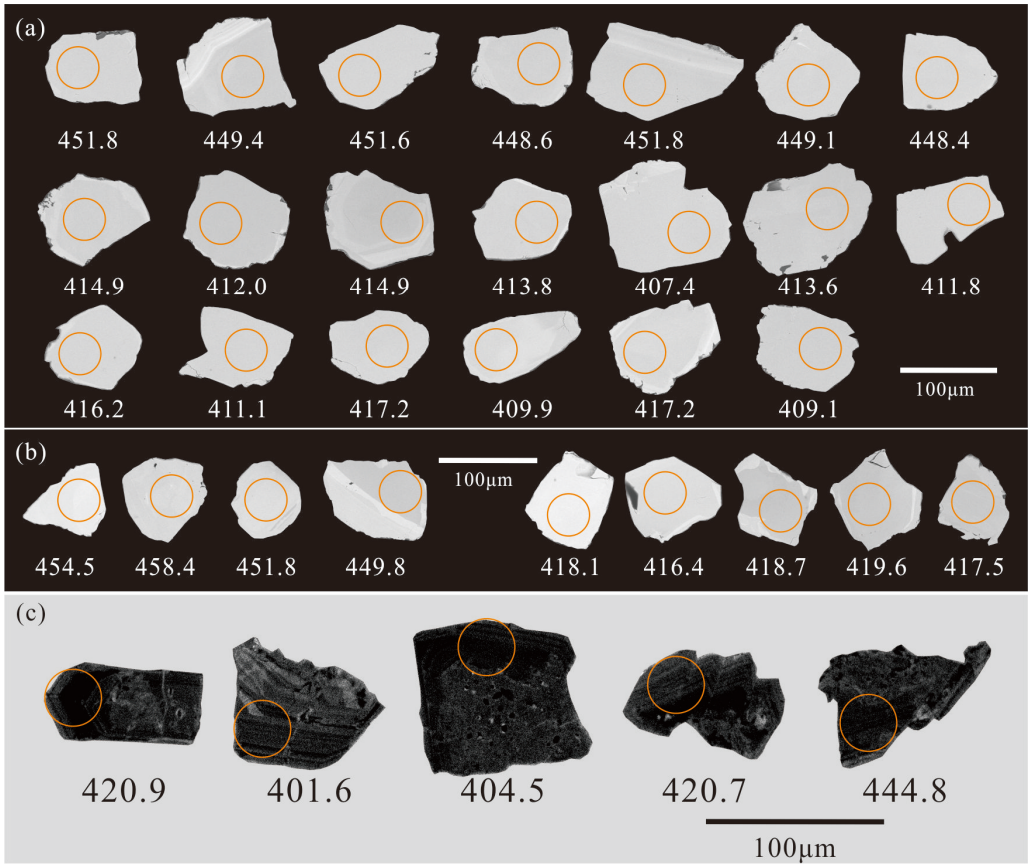


Figure 6. SEM-back-scattered electron (BSE) and Cathodoluminescence (CL) images of CGMs and zircons from the Tashidaban granitic pegmatite Li deposit. (**a**) CGMs from the aplite zone of ρ40 elbaite pegmatite; (**b**) CGMs from the aplite zone of ρ36 spodumene pegmatite; (**c**) Zircons from ρ26 tourmaline granite. The orange circles denote the U-Pb dating sites.

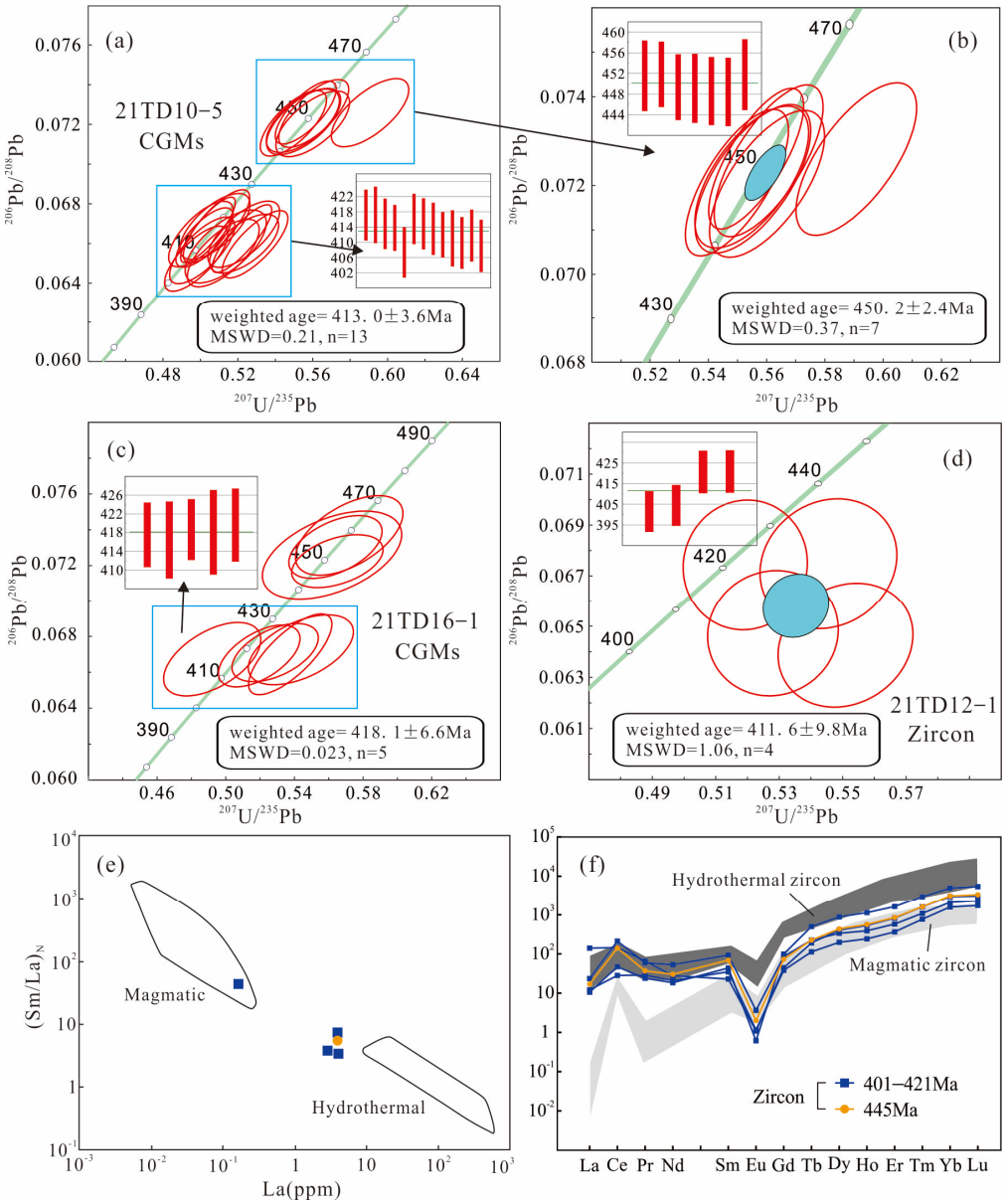


Figure 7. Diagrams of CGMs and zircons from the Tashidaban granitic pegmatite Li deposit. (**a**,**b**) CGMs from the zone of ρ40 elbaite pegmatite; (**c**) CGMs from the zone of ρ36 spodumene pegmatite; (**d**) Zircons from the zone of ρ26 tourmaline granite; (**e**) Chondrite-normalized [76] discrimination plots of $(Sm/La)_N$ vs. La; (**f**) Chondrite-normalized REE concentrations for magmatic and hydrothermal zircon [77].

The CGM grains from ρ36 spodumene pegmatite are mainly black and subhedral (Figures 5g and 6b). Four analyzed points (Sample number 21TD16-1) vary from 458 to 450 Ma, and five analyzed points have a weighted mean $^{206}Pb/^{238}U$ age of 418.1 ± 6.6 Ma (1σ; MSWD = 0.023), varying from 420 to approximately 416 Ma (Figure 7c; Table 2).

The zircon grains from ρ26 tourmaline granite are predominantly black and subhedral to anhedral with a blurred and sponge texture in few inclusions, while the rims have little oscillatory zoning (Figure 6c). One analyzed point has an older $^{206}Pb/^{238}U$ age of 445 Ma, and four points have a weighted mean $^{206}Pb/^{238}U$ age of 411.6 ± 9.8 Ma (1σ; MSWD = 1.06), varying from 421 to 402 Ma (Figure 7d; Table 3).

Table 2. Concentrations of U, Th, and Pb, and U-Pb isotopes of CGMs from the ρ40 elbaite pegmatite and the ρ36 spodumene pegmatite in the Tashidaban granitic pegmatite Li deposit.

No.	Pb (ppm)	Th (ppm)	U (ppm)	Th/U	$^{207}Pb/^{206}Pb$	Error (1σ)	$^{207}Pb/^{235}U$	Error (1σ)	$^{206}Pb/^{238}U$	Error (1σ)	$^{206}Pb/^{238}U$ Age (Ma)	$^{206}Pb/^{238}U$ 1sigma
21TD10-5-1	28	10	367	0.03	0.0556	0.0009	0.5566	0.0108	0.0726	0.0010	451.8	6.3
21TD10-5-2	23	9	302	0.03	0.0557	0.0010	0.5551	0.0129	0.0722	0.0011	449.4	6.3
21TD10-5-3	25	11	332	0.03	0.0562	0.0011	0.5609	0.0123	0.0726	0.0011	451.6	6.8
21TD10-5-4	24	9	323	0.03	0.0555	0.0010	0.5500	0.0117	0.0721	0.0011	448.6	6.6
21TD10-5-5	27	8	381	0.02	0.0589	0.0010	0.5910	0.0137	0.0726	0.0011	451.8	6.8
21TD10-5-6	22	10	306	0.03	0.0560	0.0012	0.5555	0.0131	0.0722	0.0011	449.1	6.6
21TD10-5-7	23	8	322	0.03	0.0565	0.0011	0.5603	0.0130	0.0720	0.0011	448.4	6.6
21TD10-5-8	22	8	323	0.02	0.0548	0.0011	0.5002	0.0115	0.0665	0.0011	414.9	6.6
21TD10-5-9	25	9	372	0.03	0.0576	0.0012	0.5236	0.0122	0.0660	0.0010	412.0	5.9
21TD10-5-10	25	10	378	0.03	0.0573	0.0012	0.5234	0.0127	0.0665	0.0011	414.9	6.7
21TD10-5-11	25	9	371	0.03	0.0551	0.0010	0.5020	0.0101	0.0663	0.0010	413.8	6.0
21TD10-5-12	20	9	307	0.03	0.0554	0.0010	0.4976	0.0112	0.0652	0.0011	407.4	6.6
21TD10-5-13	25	10	373	0.03	0.0575	0.0010	0.5225	0.0105	0.0663	0.0011	413.6	6.8
21TD10-5-14	27	11	390	0.03	0.0583	0.0010	0.5295	0.0116	0.0660	0.0011	411.8	6.8
21TD10-5-15	31	12	444	0.03	0.0550	0.0009	0.5039	0.0097	0.0667	0.0011	416.2	6.6
21TD10-5-16	16	9	235	0.04	0.0563	0.0012	0.5135	0.0144	0.0658	0.0012	411.1	7.3
21TD10-5-17	23	10	320	0.03	0.0551	0.0011	0.5077	0.0124	0.0669	0.0011	417.2	6.6
21TD10-5-18	24	10	348	0.03	0.0556	0.0010	0.5009	0.0115	0.0656	0.0011	409.9	6.7
21TD10-5-19	29	12	429	0.03	0.0552	0.0009	0.5085	0.0118	0.0669	0.0012	417.2	7.4
21TD10-5-20	30	12	454	0.03	0.0565	0.0010	0.5121	0.0127	0.0655	0.0011	409.1	6.8
21TD16-1-1	8	1	108	0.006	0.0571	0.0019	0.5642	0.0179	0.0731	0.0012	454.5	7.0
21TD16-1-2	5	0	63	0.007	0.0577	0.0023	0.5723	0.0207	0.0737	0.0015	458.4	8.8
21TD16-1-3	9	1	117	0.013	0.0572	0.0018	0.5653	0.0176	0.0723	0.0010	449.8	5.9
21TD16-1-4	4	0	52	0.007	0.0564	0.0026	0.5622	0.0268	0.0726	0.0016	451.8	9.8
21TD16-1-5	12	1	170	0.007	0.0586	0.0015	0.5379	0.0160	0.0670	0.0015	418.1	9.0
21TD16-1-6	5	1	81	0.007	0.0539	0.0019	0.4924	0.0187	0.0667	0.0014	416.4	8.2
21TD16-1-7	7	1	106	0.010	0.0584	0.0020	0.5291	0.0166	0.0671	0.0011	418.7	6.5
21TD16-1-8	5	0	73	0.006	0.0595	0.0022	0.5441	0.0202	0.0673	0.0013	419.6	7.8
21TD16-1-9	13	2	182	0.008	0.0565	0.0015	0.5198	0.0157	0.0669	0.0011	417.5	6.9

Table 3. Concentrations of U, Th, and Pb, and U-Pb isotopes of zircons from ρ26 tourmaline granite in the Tashidaban granitic pegmatite Li deposit.

No.	Pb (ppm)	Th (ppm)	U (ppm)	Th/U	$^{207}Pb/^{206}Pb$	Error (1σ)	$^{207}Pb/^{235}U$	Error (1σ)	$^{206}Pb/^{238}U$	Error (1σ)	$^{206}Pb/^{238}U$ Age (Ma)	$^{206}Pb/^{238}U$ 1sigma
21TD12-1-1	745	89	11,102	0.01	0.0587	0.0013	0.5457	0.0143	0.0675	0.0017	420.9	10.2
21TD12-1-2	441	51	6628	0.01	0.0622	0.0013	0.5511	0.0140	0.0643	0.0016	401.6	9.8
21TD12-1-3	690	153	10,479	0.01	0.0592	0.0012	0.5282	0.0136	0.0648	0.0016	404.5	9.8
21TD12-1-4	777	131	11,434	0.01	0.0559	0.0011	0.5194	0.0129	0.0674	0.0017	420.7	10.2
21TD12-1-5	374	27	5140	0.01	0.0585	0.0014	0.5762	0.0163	0.0714	0.0018	444.8	10.9

5.2. Mineral Chemistry of Zircon

The Th/U ratios of both zircons from ρ26 tourmaline granite are 0.01 (Table 3). In the chondrite-normalized REE (rare-earth element) diagrams of tourmaline granite, the samples are distinguished by their enrichment in both LREE (light rare-earth elements) and HREE (heavy rare-earth elements) (Figure 7f, Table 4). These samples exhibit positive Ce anomalies and negative Eu anomalies. In the $(Sm/La)_N$ vs. La magmatic and hydrothermal zircon discrimination plot [77], one zircon grain was plotted in the magmatic zircon field, and three grains were plotted between the magmatic and hydrothermal zircon fields (Figure 7e).

Table 4. Concentrations (ppm) of rare-earth element (REE) in zircons from ρ26 tourmaline granite in the Tashidaban granitic pegmatite Li deposit.

No.	La	Ce	Pr	Nd	Sm	Eu	Gd	Tb	Dy	Ho	Er	Tm	Yb	Lu
21TD12-1-1	43.57	116.75	8.03	16.75	4.47	0.08	11.50	9.04	130.69	38.42	172.96	51.83	629.11	100.41
21TD12-1-2	7.31	170.89	7.22	31.89	18.18	0.27	22.13	10.69	108.32	27.90	121.76	35.29	438.22	74.28
21TD12-1-3	3.28	38.19	2.93	11.07	8.52	0.05	25.66	23.68	283.88	81.51	341.32	97.00	1042.24	174.87
21TD12-1-4	3.77	22.86	3.53	12.54	6.83	0.09	9.90	5.35	63.71	17.40	76.58	25.02	330.04	55.86
21TD12-1-5	5.30	113.99	4.50	18.12	13.49	0.15	18.95	10.68	140.15	40.70	178.51	52.01	656.11	108.85

5.3. Whole-Rock Geochemical Data

Whole-rock geochemical data are listed in Supplementary Table S1. The granite rock facies in the Kumudaban area are composed of biotite granite, muscovite granite, albite granite, and tourmaline granite, with relatively elevated SiO_2 (69.59–75.03%), Al_2O_3 (14.80–15.49%), and Na_2O (3.69–5.75%) contents, and lower TiO_2 content ranging from 0.01% to 0.39%. The A/CNK values range from 1.11 to 1.40 with differentiation index (DI) ranging from 81.87 to 93.62 increasing from biotite granite to tourmaline granite. In the chondrite-normalized diagram (Figure 8a), biotite granite exhibits a rightward-shaped pattern of light rare-earth element (LREE) enrichment ($(La:Yb)_N$ = 46.88 to 50.21), while the others show relatively flat distribution trends ($(La:Yb)_N$ = 0.20 to 3.76). All samples except biotite granite exhibit significant negative Eu anomalies (δEu = 0.07 to 0.40), and the total rare-earth element (REE) content decreases from biotite granite (average ΣREE = 177.88) to tourmaline granite (average ΣREE = 10.77). In the spider diagram (Figure 8b), all samples except biotite granite show depletions in Ba and Ti.

The fine-grained aplite sample of the spodumene pegmatite (448 Ma) in the Tamuqie granitic pegmatite Li deposit has relatively low SiO_2 content (average 68.58%), higher Al_2O_3 (average 17.89%), and Na_2O content (average 9.39%), with an average A/CNK value of 1.12 and average DI value of 95.70. The total REE content is lower than that of the Kumudaban granite (average ΣREE = 3.02) (Figure 8a).

The tourmaline granite samples compared to the aplite samples of elbaite pegmatite and spodumene pegmatite in the Tashidaban granitic pegmatite Li deposit have relatively high SiO_2 content (average 73.36%) and low Al_2O_3 content (average 15.34%), with an average A/CNK value of 1.20. The fine-grained aplite zone of the ρ36 spodumene pegmatite exhibits the highest A/CNK values (average 1.57) and the lowest total REE content (average ΣREE = 0.54) (Figure 8a). The average DI value of tourmaline granite, elbaite pegmatite, and spodumene pegmatite ranged from 95.09 to 98.13. Furthermore, in the spider diagram, the pegmatitic granite samples exhibit similar distribution patterns (Figure 8b).

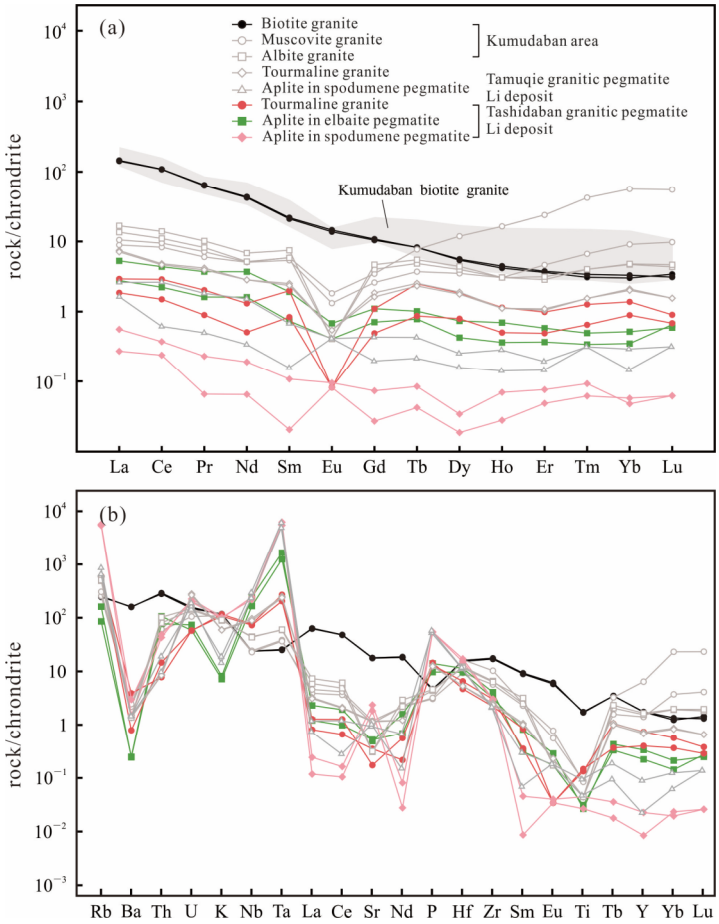


Figure 8. (**a**) Chondrite-normalized REE patterns [78] and (**b**) primitive mantle-normalized trace element diagrams [76]. Kumudaban biotite granite are from [65].

6. Discussion

6.1. Formation Times of the Tashitaban Li Granitic Pegmatites

The CGMs found in the granitic pegmatite contain relatively low common Pb contents and exhibit suitable Th and U contents for U-Pb geochronology [79,80]. Reflected light and BSE images show that most samples of CGMs are homogeneous. Only a few images exhibit bright Ta-Mn oscillatory zoning within dark Mn-rich cores, which indicates that these samples have not undergone hydrothermal metasomatism [81,82]. The ages of CGMs of ρ40 elbaite pegmatite are primarily distributed in two intervals with ranges from 452 to 448 Ma and 417 to 407 Ma. Additionally, those of ρ36 spodumene pegmatite range from 458 to 450 Ma and 420 to 416 Ma. Since the restriction of CGMs stability, the problem of inheritance from precursor rocks can be ruled out [79]. A similar phenomenon showing in a single pegmatite was reported by Melcher et al. [83] and Konzett et al. [84], which have a large age spread of 150–309 Ma in Passeier Valley (Italy) and 70–172 Ma age spread in Eastern Alpine (Italy). Konzett et al. [84] suggested that the oldest CGMs age represents the emplacement age and the age spread due to Cretaceous resetting involves multiple tectono-magmatic events. However, the two distribution interval ages in the single pegmatite of the Tashidaban granitic pegmatite Li deposit possibly represent two independent tectonic thermal events. In the Tashisayi granitic pegmatite Li deposit, three-stage age distribution was found in a composited aplite–pegmatite dike at 472 Ma, 440 Ma, and 416 Ma, with the oldest age originating from the Lep-Ab-Qz pegmatite and the middle age from the Spd-Ab-Qz pegmatite [65]. Additionally, Li-Be mineralization events were found to occur during 472—455 Ma in the North Tugeman granitic pegmatite Li-Be deposit and superimposed by 436–435 Ma and 415 Ma fine-grained granite [46].

In this study, only five age data points are considered reliable, among which the oldest age is 445 Ma, and the other four ages range between 421 and 402 Ma with weighted average age of 411.6 ± 9.8 Ma (MSWD = 1.06). Cores of zircon grains in the ρ26 tourmaline granite are predominantly black and exhibit a blurred and sponge texture with few inclusions, while the rims have little oscillatory zoning (Figure 6c), which indicates that the zircon grains originated from magmatic sources but underwent later recrystallization or metamorphic events [85]. Furthermore, the Th/U ratios of four zircons are 0.1, which are lower than typical magmatic zircons [86]. In the chondrite-normalized REE diagrams, the samples exhibit a similar pattern to hydrothermal zircons (Figure 7f). In the $(Sm/La)_N$ vs. La magmatic and hydrothermal zircon discrimination plot [77], three grains were plotted between the magmatic and hydrothermal zircon fields (Figure 7e). Combined with the CL features, these geochemical characteristics suggest that the zircons have undergone late-stage metamorphic alteration.

The alteration phenomena observed in this study indicate that the pegmatites in the Tashidaban granitic pegmatite Li deposit have undergone a later magmatic–hydrothermal event. The undulose extinction coarse-grained quartz intergrown with spodumene and albite undergoes recrystallization at the edges into granoblastic quartz, which is commonly observed in ρ40 elbaite pegmatite and ρ36 spodumene pegmatite (Figure 5b,h,i). These characteristics represent the synkinematic emplacement of the pegmatites, which are restricted to the shear zones [87]. The Altun region was undergoing simultaneous compression and amalgamation of three micro-continental blocks, resulting in intense compression and the formation of shear zones from the north and south at ~450 Ma (see Section 6.3). Moreover, elbaite was observed being replaced by a later fine-grained albite granite (Figure 5c). The replacement of aplite zone by late-stage fine-grained albite granite can be observed in Figure 5a, and both the aplite zone and albite granite have CGMs intergrown with albite and quartz, while the Spd-Ab-Qz zone is replaced by late-stage fine-grained muscovite albite granite in the ρ36 spodumene pegmatite (Figure 5i). All indicate that the pegmatites in the Tashidaban granitic pegmatite Li deposit have undergone the superimposition of a later magmatic–hydrothermal event. Therefore, the Li-mineralization age of the Tashidaban granitic pegmatite Li deposit is 450.2 ± 2.4 Ma, with superimposing of a late-stage magmatic–hydrothermal event during 418–412 Ma.

Multiple episodes of subduction–collision events occurred on both the northern and southern sides of the CAB due to a complex tectonic evolution in the Early Paleozoic. Statistical results indicate that Early Paleozoic magmatic granitoids in the North Altun Block (NAB) were formed between 514 and 411 Ma, while granitoids in the CAB are concentrated between 522 and 432 Ma. Furthermore, Wang et al. [88] obtained an age of 417 Ma from leucosome in garnet-bearing biotite gneiss of the Altun Group. An age of 413.8 ± 7.4 Ma from muscovite Ar-Ar dating of the Suwushijie monzogranite [68] as well as ages of 406–405 Ma from diorite and granite dykes in the Tashsayi area [89] were obtained. It indicates that contemporaneous magmatic activities exist in the Central Altun during 417–405 Ma. The ages of rare-metal pegmatite in CAB are shown in Figure 9. Ages obtained from the Tashidaban Li granitic pegmatites range in two intervals: 450.2 ± 2.4 Ma and 418–412 Ma, which are consistent with the regional magmatic and mineralization events.

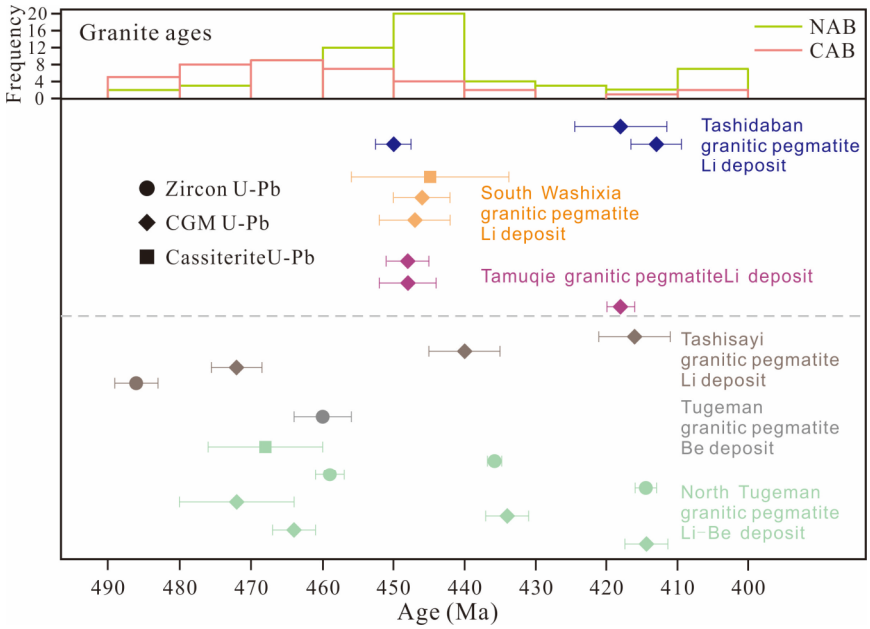


Figure 9. Formation times of granites and granitic pegmatite Li-Be deposits in the CAB. The granite ages of the NAB are from [90–101]; the granite ages of the CAB are from [46–48,60,62,88–90,102–105]. Igneous crystallization and mineralization ages of Li-Be deposits are consistent with the literature in Figure 1.

6.2. Petrogenesis of the Kumudaban Granitoids and Origin of Tashitaban Granitic Pegmatites

6.2.1. Petrogenesis of the Kumudaban Granitoids

An S-type granitoid is generally considered as a peraluminous granitoid, which is mainly formed by the partial melting of crustal materials [106,107]. The Kumudaban granitoid samples, with Alumina saturation index (ASI) values exceeding 1.1, are classified as peraluminous granite (Figure 10a). The content of corundum in granitoid samples in Cross, Iddings, Pirrson, and Washington (CIPW) norm calculation are more than 1%. Muscovite and garnet are identified under the microscope observation (Figure 3b–d). In addition, apatite commonly crystallizes early in I- and A-type granitic magma, resulting in a decrease in the P_2O_5 content of the residual magma. This decrease establishes a strong negative correlation with the SiO_2 content, while, P_2O_5 in S-type granite increases or basically remains unchanged with the increase in SiO_2 [108–110]. P_2O_5 values in these samples are basically unchanged with increased SiO_2 (except for tourmaline granite, with P_2O_5 in the range 0.07~0.09). The Kumudaban granitoids were characterized as S-type high-K to calc-alkaline granite plotting in the area of the high-K to calc-alkaline series (biotite granites to muscovite granites to albite granites, tourmaline granites) (Figure 10b) [111,112].

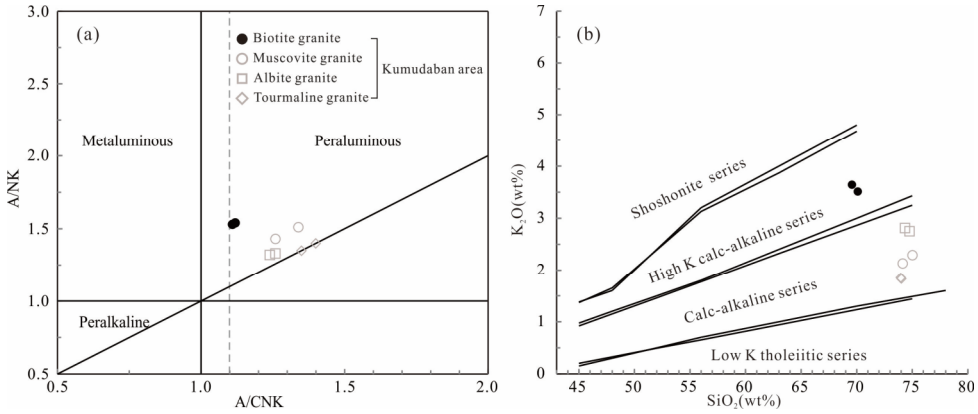


Figure 10. (**a**) ASI shown by A/NK vs. A/CNK diagram [113]; (**b**) the K_2O vs. SiO_2 diagram with dividing curves from [114].

6.2.2. Origin of the Tashidaban Li Granitic Pegmatites

Two petrogenetic processes were proposed to explain the formation of rare-element pegmatites: (1) extensive fractionation of fertile parental granitic magma [115–118], and (2) partial melting of rare-element-rich source rocks [119–121]. The large granite plutons near the Tashidaban granitic pegmatite Li deposit are the Kumudaban granite pluton (with zircon U-Pb ages 445–451 Ma) and the Suwushijie intermediate-acidic pluton (with zircon U-Pb ages 464–475 Ma). In this study, the Li-mineralizition age in the Tashidaban granitic pegmatite Li deposit is 450.2 ± 2.4 Ma. The Tashidaban Li granitic pegmatites should originate from the highly crystallized differentiation of the Kumudaban biotite granite pluton (Suwushijie intermediate-acidic pluton is excluded due to the presence of a >6 Ma age gap). The Tamuqie granitic pegmatite Li deposit is located north of the Tashidaban granitic pegmatite Li deposit and has a Li-mineralization age of 448 Ma with occurrence of a 418 Ma tourmaline-bearing albite pegmatite. Since pegmatites accentuate the trace element signatures of their granitic sources [24,25], the chemical evolution of Tashidaban Li granitic pegmatites should be similar to the Tamuqie spodumene pegmatite.

Zr/Hf ratio is a useful index of the extent of fractional crystallization of a felsic melt [122,123]. The element pairs K/Rb, K/Cs, and Nb/Ta typically exhibit synergistic behavior, and their variation mechanisms are similar [124]. This also suggests that these ratios could be indicators of the degree of differentiation of felsic melts [27,125]. The pairs mentioned above were plotted against Zr/Hf, which shows a well-defined evolutionary trend in the Kumudaban granite rock facies (Figure 11). The biotite granite exhibits the highest K/Rb, K/Cs, and Nb/Ta ratios. The gradual decrease in these ratios from muscovite granite to albite granite and tourmaline granite shows a clear trend in magmatic evolution. With ongoing of magmatic evolution, the ratios of these incompatible and compatible elements pair decrease successively from tourmaline granite to elbaite pegmatite to spodumene pegmatite in the Tashidaban granitic pegmatite Li deposit (Figure 11). Samples from the aplite zone in spodumene pegmatite (448 Ma) in the Tamuqie granitic pegmatite Li deposit and the aplite zone in ρ36 spodumene pegmatite in the Tashidaban granitic pegmatite Li deposit almost overlap (Figure 11). The similar distributions of trace elements (Figure 8) indicate a comparable chemical evolution of the granitic magma. The trace element distribution in the normalized chondrite and primitive mantle-normalized diagram have similar patterns, and total REE content shows a continuous decrease trend (Figure 8). All mentioned above indicate that the Tashidaban Li granitic pegmatites have a close petrogenetic relationship with Kumudaban granite pluton. Another interpretation suggests that the petrogenetic processes of the Li granitic pegmatites originate from the low-degree partial melting of metamorphic rocks. This mode of origin was confirmed to explain some rare-metal granitic pegmatite deposits worldwide [84,126]. However, no evidence of migmatization was found within the Tashidaban granitic pegmatite Li deposit [102], and no metamorphic minerals such as kyanite and chlorite were discovered in

the pegmatite [127,128]. Thus, the evidence above suggests that the Tashidaban Li granitic pegmatites originated from extensive fractionation of the Kumudaban granite pluton.

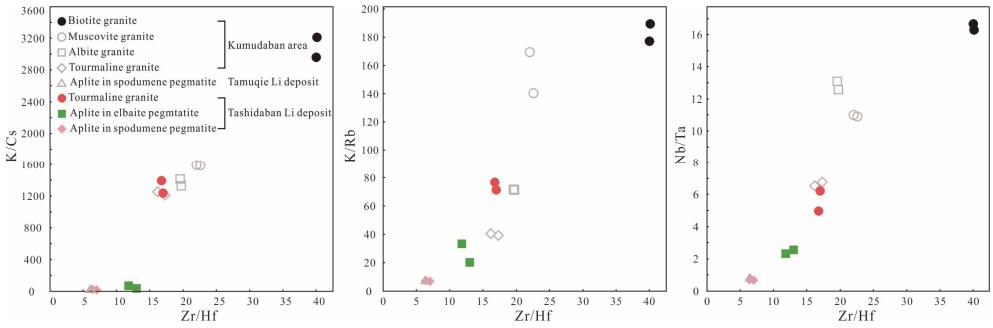


Figure 11. Selected variation diagrams of granites and pegmatites from the Kumudaban area, Tamuqie granitic pegmatite Li deposit, and Tashidaban granitic pegmatite Li deposit.

6.3. Geodynamic Setting of the Tashitaban Li Granitic Pegmatite Deposit

The Central Altun orogenic system is a product of the amalgamation of multiple micro-continental blocks and island arcs [129]. This complex system originated from subduction–accretion–collision processes in the Proto-Tethys Ocean during the Early Paleozoic [130,131].

The existence of supra-subduction zone (SSZ) ophiolite and plagiogranite are evident of the North Altun ocean subducted from north to south under the CAB with the indication of the initial subduction before ~521–512 Ma [56,132,133]. A series of high-temperature–low-pressure (HP–LT) metamorphic rocks (blueschists, eclogites: ages in 491–520 Ma) [134,135] and related magmatism events (arc volcanic rocks and I- and S-type granites) were formed with ongoing subduction [92–94,136–142]. Zircon age reveals these volcanic rocks and granites were formed between 517 and 459 Ma, which is coeval with the age spectra of detrital zircons in the Early Paleozoic sedimentary rocks from the North Altun [143]. A series of syn-collisional granite formed in the thickened lower crust at 458–431 Ma indicated a collisional regime [92–94,96,97,99]. The transition of the tectonic regime has changed to extension at ~425 Ma with the characterizations of low Sr, Sr/Y and $(La/Yb)_N$ granitoids (425–410 Ma) [94,96,99].

The high-pressure (HP)–ultrahigh-pressure (UHP) belt is located south of the Central Altun block, specifically in the Jianggalesayi, Danshuiquan, and Yinggelisayi areas. This belt comprises various rock types, including UHP eclogite, garnet (Grt) pelitic gneisses, Grt clinopyroxenite, Grt granite gneisses, and Grt peridotite. [144–147]. Systematic study of the P-T-t evolution and zircon age in HP-UHP metamorphic rocks inferred three phases of metamorphism corresponding to the continental deep subduction (~509–490 Ma) and rollback of the subducting slab (~490–440 Ma) [148,149]. Extensive magmatism was triggered by this, and consequently granitoids were formed between 522 and 432 Ma, with to the I- and S-type affinities [46–48,59–62,88,89,102–105]. The tectonic regime has changed to extension in South of the Central Altun block after 432 Ma, which is characterized by intraplate granites (432–418 Ma) [66,150], bimodal volcanic rocks (406 Ma) [151], and A-type granites (432–385 Ma) [152–154].

The Li-mineralization age of the Tashidaban granitic pegmatite Li deposit is 450.2 ± 2.4 Ma with superimposition of the late-stage magmatic–hydrothermal event that occurred at 418 to 412 Ma. The Central Altun block experienced intense continental collision between 450 and 445 Ma due to the substantial crustal thickening and regional Barrovian metamorphism [155]. This led to extensive dehydration melting of biotite under granulite facies and generating voluminous granitic magmas, which subsequently crystallized and differentiated to form the Kumudaban to Tatebulake large syn-kinematic biotite granite plutons [60,62,102]. The Tamuqie and Tashidaban Li granitic pegmatites were formed during this period through extreme differentiation by fractional crystallization of granitic magma. The collision ceased on both the northern and southern sides after 432 Ma, and extensional tectonic settings led to lithospheric delamination leading to the lower

crust triggered mantle-derived magmatism, resulting in the emplacement of granitic magmas, superimposing the Tashidaban granitic pegmatite Li deposit at 418–412 Ma.

7. Conclusions

Multiple episodes of rare-metal Li-Be mineralization events occurred in the Central Altun during the Early Paleozoic. A newly discovered Tashidaban granitic pegmatite Li deposit, at the northern margin of the Central Altun Block, hosts three distinct types of granitic pegmatities: tourmaline-bearing albite pegmatite, elbaite pegmatite, and spodumene pegmatite. These uniformed pegmatites intruded into the two-mica schist and marble of the Muzisayi Formation of the Tashidaban Group. CGMs and zircon U-Pb dating results reveal the Li-mineralization age of the Tashidaban granitic pegmatite Li deposit is 450.2 ± 2.4 Ma, with a superimposed late-stage magmatic–hydrothermal event occurring at 418 to 412 Ma. The whole-rock geochemical results indicate that the Kumudaban granitoids belongs to the S-type high-K to calc-alkaline granite, and the Tashidaban Li granitic pegmatites have originated from the extreme differentiation by fractional crystallization of the Kumudaban granite pluton.

Supplementary Materials: The following supporting information can be downloaded at: https://www.mdpi.com/article/10.3390/min14060542/s1, Supplementary Table S1: Major element (wt%) and trace element (ppm) geochemistry of the granites and pegmatites from Kumudaban area, Tamuqie granitic pegmatite Li deposit and Tashidaban granitic pegmatite Li deposit.

Author Contributions: Conceptualization, X.X. and K.K.; methodology, X.X. and H.L.; software, Z.L. and K.K.; validation, K.K.; investigation, K.K., X.W. and L.N.; writing—original draft preparation, K.K.; writing—review and editing, Y.M.; visualization, X.X.; supervision, H.L.; project administration, P.Z., J.C. and X.L.; funding acquisition, X.X. All authors have read and agreed to the published version of the manuscript.

Funding: This research was jointly supported by the National Natural Science Foundation of China (Grant Number 42250202, 42272075) and Extreme Geological Events Team (2021ZT09H399), second comprehensive scientific investigation of the Qinghai-Tibet Plateau (Grant Number 2019QZKK0802).

Data Availability Statement: At the request of other researchers, the authors of the article can provide the original data.

Acknowledgments: We are indebted to Xiangjing Yu and Huiwen Wang for sample preparation, as well as to Shuangrong Zhang and Huan Hu for laboratory assistance. We also express our gratitude to the four anonymous reviewers for their constructive suggestions, and Chen Zhao for revising the expression of the article.

Conflicts of Interest: Peng Zhang, Xingzhong Liu and Jianzhong Chen are employees of No. 3 Geological Party, Xinjiang Bureau of Geology and Mineral Exploration and Development, Korla, Xinjiang 841000, China. Lei Niu is employee of Exploration and Development Research Institute, Zhongyuan Oilfield Company, SINOPEC, Puyang 457001, China. The paper reflects the views of the scientists and not the company.

References

1. Schulz, K.J.; DeYoung, J.H.; Seal, R.R.; Bradley, D.C. *Critical Mineral Resources of the United States: Economic and Environmental Geology and Prospects for Future Supply*; U.S. Geological Survey: Reston, VA, USA, 2017; 797p. [CrossRef]
2. Zhai, M.G.; Wu, F.Y.; Hu, R.Z.; Jiang, S.Y.; Li, W.C.; Wang, R.C.; Wang, D.H.; Qi, T.; Qin, K.Z.; Wen, H.J. Critical metal mineral resources: Current research status and scientific issues. *Bull. Natl. Nat. Sci. Found. China* **2019**, *2*, 106–111. (In Chinese with English abstract)
3. Hou, Z.Q.; Chen, J.; Zhai, M.G. Current status and frontiers of research on critical mineral resources. *Chin. Sci. Bull.* **2020**, *65*, 3651–3652. (In Chinese with English abstract) [CrossRef]
4. Jaskula, B.W. *Beryllium: U.S. Geological Survey Mineral Commodity Summaries*; U.S. Geological Survey: Reston, VA, USA, 2013; pp. E1–E32. [CrossRef]
5. Linnen, R.L.; Van Lichtervelde, M.; Černý, P. Granitic pegmatites as sources of strategic metals. *Elements* **2012**, *8*, 275–280. [CrossRef]

6. Roda-Robles, E.; Villaseca, C.; Pesquera, A.; Gil-Crespo, P.P.; Vieira, R.; Lima, A.; Garate-Olave, I. Petrogenetic relationships between Variscan granitoids and Li-(FP)-rich aplite-pegmatites in the Central Iberian Zone: Geological and geochemical constraints and implications for other regions from the European Variscides. *Ore Geol. Rev.* **2018**, *95*, 408–430. [CrossRef]
7. Roda-Robles, E.; Vieira, R.; Lima, A.; Errandonea-Martin, J.; Pesquera, A.; Cardoso-Fernandes, J.; Garate-Olave, I. Li-rich pegmatites and related peraluminous granites of the Fregeneda-Almendra field (Spain-Portugal): A case study of magmatic signature for Li enrichment. *Lithos* **2023**, *452*, 107195. [CrossRef]
8. Xu, Z.Q.; Zhu, W.B.; Zheng, B.H.; Shu, L.S.; Li, G.W.; Che, X.D.; Qin, Y.L. New energy strategy for lithium resource and the continental dynamics research: Celebrating the centenary of the School of Earth Sciences and Engineering, Nanjing University. *Acta Geol. Sin.* **2021**, *95*, 2937–2954.
9. Qin, K.Z.; Zhou, Q.F.; Zhao, J.X.; He, C.T.; Liu, X.C.; Shi, R.Z.; Liu, Y.C. Be-rich mineralization features of Himalayan leucogranite belt and prospects for lithium-bearing pegmatites in higher altitudes. *Acta Geol. Sin.* **2021**, *95*, 3146–3162. (In Chinese with English abstract)
10. Zhang, D.; Peng, J.; Coulson, I.M.; Hou, L.H.; Li, S.J. Cassiterite U–Pb and muscovite40Ar–39Ar age constraints on the timing of mineralization in the Xuebaoding Sn–W–Be deposit, western China. *Ore Geol. Rev.* **2014**, *62*, 315–322. [CrossRef]
11. Zhou, Q.F.; Qin, K.Z.; Tang, D.M.; Tian, Y.; Cao, M.J.; Wang, C.L. Formation Age and Evolution Time Span of the Koktokay No. 3 Pegmatite, A ltai, NW China: Evidence from U–Pb Zircon and 40Ar–39Ar Muscovite Ages. *Resour. Geol.* **2015**, *65*, 210–231. [CrossRef]
12. Zhou, Q.F.; Qin, K.Z.; Tang, D.; Wang, C.L.; Asamiah Sakyi, P. LA-ICP-MS U–Pb zircon, columbite-tantalite and 40Ar–39Ar muscovite age constraints for the rare-element pegmatite dykes in the Altai orogenic belt, NW China. *Geol. Mag.* **2018**, *155*, 707–728. [CrossRef]
13. Yan, Q.H.; Qiu, Z.W.; Wang, H.; Wang, M.; Wei, X.P.; Li, P.; Zhang, R.Q.; Li, C.Y.; Liu, J.P. Age of the Dahongliutan rare metal pegmatite deposit, West Kunlun, Xinjiang (NW China): Constraints from LA–ICP–MS U–Pb dating of columbite-(Fe) and cassiterite. *Ore Geol. Rev.* **2018**, *100*, 561–573. [CrossRef]
14. Li, P.; Li, J.; Liu, X.; Li, C.; Huang, Z.B.; Zhou, F.C. Geochronology and source of the rare-metal pegmatite in the Mufushan area of the Jiangnan orogenic belt: A case study of the giant Renli Nb–Ta deposit in Hunan, China. *Ore Geol. Rev.* **2020**, *116*, 103237. [CrossRef]
15. Xiong, Y.Q.; Jiang, S.Y.; Wen, C.H.; Yu, H.Y. Granite–pegmatite connection and mineralization age of the giant Renli TaNb deposit in South China: Constraints from U–Th–Pb geochronology of coltan, monazite, and zircon. *Lithos* **2020**, *358*, 105422. [CrossRef]
16. Zhou, Q.F.; Qin, K.Z.; Tang, D.M. Mineralogy of columbite-group minerals from the rare-element pegmatite dykes in the East-Qinling orogen, central China: Implications for formation times and ore genesis. *J. Asian Earth Sci.* **2021**, *218*, 104879. [CrossRef]
17. Wang, Z.; Li, J.; Chen, Z.; Yan, Q.G.; Xiong, X.; Li, P.; Deng, J.Y. Evolution and Li Mineralization of the No. 134 Pegmatite in the Jiajika Rare-Metal Deposit, Western Sichuan, China: Constrains from Critical Minerals. *Minerals* **2021**, *12*, 45. [CrossRef]
18. Fei, G.C.; Menuge, J.F.; Li, Y.Q.; Yang, J.; Deng, Y.; Chen, C.S.; Yang, Y.F.; Yang, Z.; Qin, L.; Zheng, L.; et al. Petrogenesis of the Lijiagou spodumene pegmatites in Songpan-Garze Fold Belt, West Sichuan, China: Evidence from geochemistry, zircon, cassiterite and coltan U-Pb geochronology and Hf isotopic compositions. *Lithos* **2020**, *364*, 105555. [CrossRef]
19. Zhao, H.; Chen, B.; Huang, C.; Bao, C.; Yang, Q.; Cao, R. Geochemical and Sr–Nd–Li isotopic constraints on the genesis of the Jiajika Li-rich pegmatites, eastern Tibetan Plateau: Implications for Li mineralization. *Contrib. Mineral. Petrol.* **2022**, *177*, 4. [CrossRef]
20. Lv, Z.H.; Chen, J.; Zhang, H.; Tang, Y. Petrogenesis of Neoproterozoic rare metal granite-pegmatite suite in Jiangnan Orogen and its implications for rare metal mineralization of peraluminous rock in South China. *Ore Geol. Rev.* **2021**, *128*, 103923. [CrossRef]
21. Zhu, M.T.; Dong, Z.G.; Zhang, L.C. Volatile accumulation for the mineralization of Li–Be pegmatites in the northeastern Pamir, Western Kunlun, China. *Int. Geol. Rev.* **2022**, *65*, 1354–1371. [CrossRef]
22. Liu, C.Q.; Zhang, H. The lanthanide tetrad effect in apatite from the Altay No. 3 pegmatite, Xingjiang, China: An intrinsic feature of the pegmatite magma. *Chem. Geol.* **2005**, *214*, 61–77. [CrossRef]
23. Tang, Y.; Wang, H.; Zhang, H.; Lv, Z.H. K-feldspar composition as an exploration tool for pegmatite-type rare metal deposits in Altay, NW China. *J. Geochem. Explor.* **2018**, *185*, 130–138. [CrossRef]
24. Yin, R.; Huang, X.L.; Xu, Y.G.; Wang, R.C.; Wang, H.; Yuan, C.; Ma, Q.; Sun, X.M.; Chen, L.L. Mineralogical constraints on the magmatic–hydrothermal evolution of rare-elements deposits in the Bailongshan granitic pegmatites, Xinjiang, NW China. *Lithos* **2020**, *352*, 105208. [CrossRef]
25. Cao, R.; Gao, Y.B.; Chen, B.; Bagas, L.; Yan, S.C.; Huang, C.; Zhao, H. Pegmatite magmatic evolution and rare metal mineralization of the Dahongliutan pegmatite field, Western Kunlun Orogen: Constraints from the B isotopic composition and mineral-chemistry. *Int. Geol. Rev.* **2023**, *65*, 1224–1242.
26. Li, J.; Huang, X.L.; He, P.L.; Li, W.X.; Yu, Y.; Chen, L.L. In situ analyses of micas in the Yashan granite, South China: Constraints on magmatic and hydrothermal evolutions of W and Ta–Nb bearing granites. *Ore Geol. Rev.* **2015**, *65*, 793–810. [CrossRef]
27. Liu, C.; Wang, R.C.; Wu, F.Y.; Xie, L.; Liu, X.C.; Li, X.K.; Yang, L.; Li, X.J. Spodumene pegmatites from the Pusila pluton in the higher Himalaya, South Tibet: Lithium mineralization in a highly fractionated leucogranite batholith. *Lithos* **2020**, *358*, 105421.

28. Li, P.; Li, J.; Chen, Z.; Liu, X.; Huang, Z.B.; Zhou, F.C. Compositional evolution of the muscovite of Renli pegmatite-type rare-metal deposit, northeast Hunan, China: Implications for its petrogenesis and mineralization potential. *Ore Geol. Rev.* **2021**, *138*, 104380. [CrossRef]
29. Yan, Q.H.; Wang, H.; Chi, G.; Wang, Q.; Hu, H.; Zhou, K.L.; Zhang, X.Y. Recognition of A 600-km-Long Late Triassic Rare Metal (Li-Rb-Be-Nb-Ta) Pegmatite Belt in the Western Kunlun Orogenic Belt, Western China. *Econ. Geol.* **2022**, *117*, 213–236.
30. Chen, J.Z.; Zhang, H.; Tang, Y.; Lv, Z.H.; An, Y.; Wang, M.T.; Liu, K.; Xu, Y.S. Lithium mineralization during evolution of a magmatic–hydrothermal system: Mineralogical evidence from Li-mineralized pegmatites in Altai, NW China. *Ore Geol. Rev.* **2022**, *149*, 105058.
31. Han, J.; Chen, H.; Zhang, J.; Zhang, Y.F.; Zhang, R.Q. Age and evolution of the Nanyangshan rare-metal mineralized pegmatite revealed by cassiterite U-Pb geochronology and tourmaline chemistry. *Ore Geol. Rev.* **2022**, *150*, 105121. [CrossRef]
32. Li, J.; Liu, C.Y.; Liu, X.; Li, P.; Huang, Z.B.; Zhou, F.C. Tantalum and niobium mineralization from F-and Cl-rich fluid in the lepidolite-rich pegmatite from the Renli deposit in northern Hunan, China: Constraints of fluid inclusions and lepidolite crystallization experiments. *Ore Geol. Rev.* **2019**, *115*, 103187. [CrossRef]
33. Fei, G.C.; Menuge, J.F.; Chen, C.S.; Yang, Y.L.; Deng, Y.; Li, Y.G.; Zheng, L. Evolution of pegmatite ore-forming fluid: The Lijiagou spodumene pegmatites in the Songpan-Garze Fold Belt, southwestern Sichuan Province, China. *Ore Geol. Rev.* **2021**, *139*, 104441. [CrossRef]
34. Zhang, Z.; Jiang, Y.; Niu, H.; Qu, P. Fluid inclusion and stable isotope constraints on the source and evolution of ore-forming fluids in the Bailongshan pegmatitic Li-Rb deposit, Xinjiang, western China. *Lithos* **2021**, *380*, 105824. [CrossRef]
35. Li, J.K.; Wang, D.H.; Chen, Y.C. The Ore-forming Mechanism of the Jiajika Pegmatite-Type Rare Metal Deposit in Western Sichuan Province: Evidence from Isotope Dating. *Acta Geol. Sin. Engl. Ed.* **2013**, *87*, 91–101.
36. Zhang, X.; Zhang, H.; Ma, Z.L.; Tang, Y.; Lv, Z.H.; Zhao, J.Y.; Liu, Y.L. A new model for the granite–pegmatite genetic relationships in the Kaluan–Azubai–Qiongkuer pegmatite-related ore fields, the Chinese Altay. *J. Asian Earth Sci.* **2016**, *124*, 139–155. [CrossRef]
37. Zhou, J.S.; Wang, Q.; Xu, Y.G.; Cempirek, J.; Wang, H.; Ma, J.L.; Wei, G.J.; Huang, T.Y.; Zhu, G.H.; Zhang, L. Geochronology, petrology, and lithium isotope geochemistry of the Bailongshan granite-pegmatite system, northern Tibet: Implications for the ore-forming potential of pegmatites. *Chem. Geol.* **2021**, *584*, 120484. [CrossRef]
38. Fan, J.J.; Tang, G.J.; Wei, G.J.; Wang, H.; Xu, Y.G.; Wang, Q.; Zhou, J.S.; Zhang, Z.Y.; Huang, T.Y.; Wang, Z.L. Lithium isotope fractionation during fluid exsolution: Implications for Li mineralization of the Bailongshan pegmatites in the West Kunlun, NW Tibet. *Lithos* **2020**, *352*, 105236. [CrossRef]
39. Huang, T.; Fu, X.; Ge, L.; Zou, F.G.; Hao, X.F.; Yang, R.; Xiao, R.Q.; Fan, J.B. The genesis of giant lithium pegmatite veins in Jiajika, Sichuan, China: Insights from geophysical, geochemical as well as structural geology approach. *Ore Geol. Rev.* **2020**, *124*, 103557. [CrossRef]
40. Shen, P.; Pan, H.D.; Li, C.H.; Feng, H.X.; He, L.F.; Bai, Y.X.; Luo, Y.Q.; Suo, Q.Y.; Cap, C. Newly-recognized Triassic highly fractionated leucogranite in the Koktokay deposit (Altai, China): Rare-metal fertility and connection with the No. 3 pegmatite. *Gondwana Res.* **2022**, *112*, 24–51. [CrossRef]
41. Liu, L.; Kang, L.; Cao, Y.T.; Yang, W.Q. Early Paleozoic granitic magmatism related to the processes from subduction to collision in South Altyn, NW China. *Sci. China Earth Sci.* **2015**, *58*, 1513–1522. (In Chinese with English abstract) [CrossRef]
42. Kang, L.; Xiao, P.X.; Gao, X.F.; Xi, R.G.; Yang, Z.C. Early Paleozoic magmatism and collision orogenic process of the South Altyn. *Acta Geol. Sin.* **2016**, *90*, 2527–2550.
43. Romer, R.L.; Smeds, S.A. U-Pb columbite ages of pegmatites from Sveconorwegian terranes in southwestern Sweden. *Precambr. Res* **1996**, *76*, 15–30. [CrossRef]
44. Xu, X.W.; Li, H.; Shi, F.P.; Yao, F.J.; Chen, J.Z.; Yang, Z.Q.; Hong, T.; Ke, Q. Metallogenic characteristics and prospecting of granitic pegmatite-type rare metal deposits in the Tugeman area, Middle Altyn Tagh. *Acta Petrol. Sin.* **2019**, *35*, 3303–3316. (In Chinese with English abstract)
45. Xu, X.W.; Hong, T.; Li, H.; Niu, L.; Ke, Q.; Chen, J.Z.; Liu, S.K.; Zhai, M.G. Concept of high-temperature granite-pegmatite Li-Be metallogenic system with a primary study in the middle Altyn-Tagh. *Acta Petrol. Sin.* **2020**, *36*, 3572–3592. (In Chinese with English abstract)
46. Li, H. Lithium-Beryllium Mineralization of Granite-Pegmatite System in the Tugeman Area in the Middle of Altyn Tagh. Ph.D. Thesis, Chinese Academy of Sciences, Beijing, China, 2021. (In Chinese with English abstract).
47. Hong, T.; Zhai, M.G.; Xu, X.W.; Li, H.; Wu, C.; Ma, Y.C.; Niu, L.; Ke, Q.; Wang, C. Tourmaline and quartz in the igneous and metamorphic rocks of the Tashisayi granitic batholith, Altyn Tagh, northwestern China: Geochemical variability constraints on metallogenesis. *Lithos* **2021**, *400*, 106358. [CrossRef]
48. Gao, Y.B.; Zhao, X.M.; Bagas, L.; Wang, Y.L.; Jin, M.S.; Zhang, J.W.; Lu, L.; Gao, Y.J.; Yan, Z.Q.; Teng, J.X.; et al. Newly discovered Ordovician Li-Be deposits at Tugeman in the Altyn-Tagh Orogen, NW China. *Ore Geol. Rev.* **2021**, *139*, 104515. [CrossRef]
49. Wang, H.; Ma, H.D.; Zhang, S.; Du, X.F.; Huang, L.; Cai, M.Z.; Chen, G.W.; Zhu, B.Y.; Wang, Q.; Wang, K.Y.; et al. Discovery of the Huanglongling giant lithium pegmatite deposit in Altyn Tagh, Xinjiang, China. *Acta Petrol. Sin.* **2023**, *39*, 3307–3318. (In Chinese with English abstract) [CrossRef]
50. Xu, Z.Q.; Yang, J.S.; Zhang, J.X.; Jiang, M.; Li, H.B.; Cui, J.W. A comparison between the tectonic units on the two sides of the Altun sinistral strike-slip fault and the mechanism of lithospheric shearing. *Acta Geol. Sin.* **1999**, *73*, 193–205.

51. Liu, L. Tectonics Significance of High-Pressure Metamorohic Rocks and Ophiolites in Altun area, Xingjiang, China. Ph.D. Thesis, Chinese Academy of Sciences, Beijing, China, 1999. (In Chinese with English abstract).
52. Liu, L.; Wang, C.; Chen, D.L.; Zhang, A.D.; Liou, J.G. Petrology and geochronology of HP-UHP rocks from the South Altyn, northwestern China. *J. Asian Earth Sci.* **2009**, *35*, 232–244. [CrossRef]
53. Liu, L.; Wang, C.; Cao, Y.T.; Chen, D.L.; Kang, L.; Yang, W.Q.; Zhu, X.H. Geochronology of multi-stage metamorphic events: Constraints on episodic zircon growth from the UHP eclogite in the South Altyn, NW China. *Lithos* **2012**, *136*, 10–26. [CrossRef]
54. Wu, C.L.; Gao, Y.H.; Lei, M.; Qin, H.P.; Liu, C.H.; Li, M.Z.; Frost, B.R.; Wooden, J.L. Zircon SHRIMP U-Pb dating, Lu-Hf isotopic characteristics and petrogenesis of the Palaeozoic granites in Mangya area, southern Altun, NW China. *Acta Petrol. Sin.* **2014**, *30*, 2297–2323. (In Chinese with English abstract)
55. Wu, C.L.; Lei, M.; Wu, D.; Zhang, X.; Chen, H.J.; Li, T.X. Zircon U-Pb dating of Paleozoic granite from South Altun and response of the magmatic activity to the tectonic evolution of the Altun Orogenic Belt. *Acta Geol. Sin.* **2016**, *90*, 2276–2315. (In Chinese with English abstract)
56. Zhang, Z.C.; Guo, Z.J. Sm-Nd, Ar Isotopic and Geochemical Characteristics of Plagioclase Amphibolites in the Bashikaogong Area, Altun Tagh Mountains. *Geol. J. China Univ.* **2004**, *10*, 28. (In Chinese with English abstract)
57. Hao, J.B. Composition, Geochronology and Mesoproterozoic-Neoproterozoic Tectonic Evolution of the Central-Southern Altyn Tagh. Ph.D. Thesis, Northwest University, Xi'an, China, 2021. (In Chinese with English abstract).
58. Gehrels, G.E.; Yin, A.; Wang, X.F. Detrital-zircon geochronology of the northeastern Tibetan plateau. *Geol. Soc. Am. Bull.* **2003**, *115*, 881–896. [CrossRef]
59. Chen, B. Characteristics and zircon U-Pb dating of the Kumdaban rock mass swarm on the northern margin of the Azhong block. *Geol. China* **2007**, *34*, 270–275. (In Chinese with English abstract)
60. Cao, Y.T.; Liu, L.; Wang, C.; Yang, W.Q.; Zhu, X.H. Geochemical, zircon U-Pb dating and Hf isotope compositions studies for Tatelekebulake granite in South Altyn Tagh. *Acta Petrol. Sin.* **2010**, *26*, 3259–3271. (In Chinese with English abstract)
61. Kang, L.; Liu, L.; Cao, Y.T.; Wang, C.; Yang, W.Q.; Liang, S. Geochemistry, zircon U-Pb age and its geological significance of the gneissic granite from the eastern segment of the Tatelekebulake composite granite in the south Altyn Tagh. *Acta Petrol. Sin.* **2013**, *29*, 3039–3048. (In Chinese with English abstract)
62. Liu, C.H.; Wu, C.L.; Gao, Y.H.; Lei, M.; Qin, H.P. Age, composition, and tectonic significance of Palaeozoic granites in the Altyn orogenic belt, China. *Int. Geol. Rev.* **2016**, *58*, 131–154. [CrossRef]
63. Li, H.; Hong, T.; Liu, S.K.; Yang, Z.Q.; Ke, Q.; Ma, Y.C.; Wang, X.H.; Niu, L.; Kang, K.; Xu, X.W.; et al. Characteristics of early Paleozoic granite-pegmatite and associated lithium-beryllium mineralization in the Tugeman area, Altun orogenic system, northwestern China. *Ore Geol. Rev.* **2023**, *160*, 105603. [CrossRef]
64. Kang, K.; Hong, T.; Zhang, P.; Liu, S.K.; Yao, F.J.; Li, H.; Ma, Y.C.; Wang, X.H.; Liao, Z.X.; Niu, L.; et al. The large Li pegmatite deposits formed at final collision of a three micro-continent collage in the Central Altun Tagh, Northwest China. *Ore Geol. Rev.* 2024; *Revision Submitted to Journal*.
65. Ma, Y.C.; Xu, X.W.; Hong, T.; Jin, W.K.; Li, H.; Yang, Z.Q.; Liu, S.K.; Kang, K.; Wang, X.H.; Niu, L. Multiphase evolution of a Li-pegmatite field from the Tashisayi area, Altyn Tagh, NW China: Insights from a petrological, geochemical, and geochronological study. *Miner. Depos.* **2023**, *59*, 1–22. [CrossRef]
66. Xiao, P.X. The geological features of Suwushijie rockbody (group) in Altyn Tagh middle-zone. *Northwestern Geol.* **2003**, *36*, 14–23.
67. Liu, C.H. Temporal-Spatial Distribution and Tectonic Evolution of the Granitoids in the Altun Orogenic Belt. Ph.D. Thesis, Chinese Academy of Geological Science, Beijing, China, 2014. (In Chinese with English abstract).
68. Sobel, E.R.; Arnaud, N. A possible middle Paleozoic suture in the Altyn Tagh, NW China. *Tectonics* **1999**, *18*, 64–74. [CrossRef]
69. Gao, Y.B.; Zhao, X.M.; Wang, B.; Zhang, J.W.; Jin, M.S.; Yang, S.F.; Yan, Z.Q.; Teng, J.X.; Zhao, H.B.; Chao, Y.Y. Geological characteristics of fluorite deposits and ore-controlling granites, and prospecting potential of the super-large Kaerqiaer-Kumutashi fluorite mineralization belt in West Altyn-Tagh, China. *China Geol.* **2022**, *50*, 1–32. (In Chinese with English abstract)
70. Zhang, L.; Jiang, S.Y.; Romer, R.L.; Zhang, H.X.; Wan, S.L. Characteristics and formation of rare-metal pegmatites and granites in the Duanfengshan-Guanyuan district of the northern Mufushan granite complex in South China. *Lithos* **2024**, *474*, 107579. [CrossRef]
71. Xu, Z.Q.; Zheng, B.H.; Zhu, W.B.; Chen, Y.J.; Li, G.W.; Gao, J.G.; Che, X.D.; Zhang, R.Q.; Wei, H.Z.; Li, W.Q.; et al. Geologic scenario from granitic sheet to Li-rich pegmatite uncovered by Scientific Drilling at the Jiajika lithium deposit in eastern Tibetan Plateau. *Ore Geol. Rev.* **2023**, *161*, 105636. [CrossRef]
72. Melcher, F.; Sitnikova, M.A.; Graupner, T.; Nicola, M.; Thomas, O.; Friedhelm, H.K.; Eike, G.; Axel, G.; Helene, B.; Don, W.D.; et al. Fingerprinting of conflict minerals: Columbite-tantalite ('coltan') ores. *SGA News* **2008**, *23*, 1–14.
73. Che, X.D.; Wu, F.Y.; Wang, R.C.; Axel, G.; Ji, W.Q.; Zhao, Z.H.; Yang, J.H.; Zhu, Z.Y. In situ U-Pb isotopic dating of columbite-tantalite by LA-ICP-MS. *Ore Geol. Rev.* **2015**, *65*, 979–989. [CrossRef]
74. Thompson, J.; Meffre, S.; Danyushevsky, L. Impact of air, laser pulse width and fluence on U-Pb dating of zircons by LA-ICPMS. *J. Anal. At. Spectrom.* **2018**, *33*, 221–230. [CrossRef]
75. Ludwig, K.R. *ISOPLOT 3.00: A Geochronological Toolkit for Microsoft Excel*; Special Publication; Berkeley Geochronology Center: Berkeley, CA, USA, 2003; Volume 4, pp. 1–71.
76. Sun, S.S.; McDonough, W.F. Chemical and isotopic systematics of oceanic basalts: Implications for mantle composition and processes. *Geol. Soc. Lond. Spec. Publ.* **1989**, *42*, 313–345. [CrossRef]

77. Hoskin, P.W.O. Trace-element composition of hydrothermal zircon and the alteration of Hadean zircon from the Jack Hills. *Australia. Geochim. Cosmochim. Acta* **2005**, *69*, 637–648. [CrossRef]
78. McDonough, W.F.; Sun, S.S. The composition of the Earth. *Chem. Geol.* **1995**, *120*, 223–253. [CrossRef]
79. Romer, R.L.; Wright, J.E. U-Pb dating of columbites: A geochronologic tool to date magmatism and ore deposits. *Geochim. Cosmochim. Acta* **1992**, *56*, 2137–2142. [CrossRef]
80. Baumgartner, R.; Romer, R.L.; Moritz, R.; Sallet, R.; Chiaradia, M. Columbite–tantalite-bearing granitic pegmatites from the Seridó Belt, northeastern Brazil: Genetic constraints from U–Pb dating and Pb isotopes. *Can. Mineral.* **2006**, *44*, 69–86. [CrossRef]
81. Linnen, R.L.; Cuney, M. Granite-related rare-element deposits and experimental constraints on Ta-Nb-W-Sn-Zr-Hf mineralization. In *Rare-Element Geochemistry and Mineral Deposits*; Linnen, R.L., Samson, I.M., Eds.; Geological Association of Canada, GAC (Short Course): St. John's, NF, Canada, 2005.
82. Badanina, E.V.; Sitnikova, M.A.; Gordienko, V.V.; Melcher, F.; Gäbler, H.E.; Lodziak, J.; Syritso, L.F. Mineral chemistry of columbite-tantalite from spodumene pegmatite of Kolmozero, Kola Peninsula (Russia). *Ore Geol. Rev.* **2015**, *64*, 720–735. [CrossRef]
83. Melcher, F.; Graupner, T.; Gäbler, H.E.; Sitnikova, M.; Oberthür, T.; Gerdes, A.; Badanina, E.; Chudy, T. Mineralogical and chemical evolution of tantalum–(niobium–tin) mineralisation in pegmatites and granites. Part 2: Worldwide examples (excluding Africa) and an overview of global metallogenetic patterns. *Ore Geol. Rev.* **2017**, *89*, 946–987. [CrossRef]
84. Konzett, J.; Schneider, T.; Nedyalkova, L.; Hauzenberger, C.; Melcher, F.; Gerdes, A.; Whitehouse, M. Anatectic granitic pegmatites from the Eastern Alps: A case of variable rare-metal enrichment during high-grade regional metamorphism–I: Mineral assemblages, geochemical characteristics, and emplacement ages. *Can. Mineral.* **2018**, *56*, 555–602. [CrossRef]
85. Geisler, T.; Schaltegger, U.; Tomaschek, F. Re-equilibration of zircon in aqueous fluids and melts. *Elements* **2007**, *3*, 43–50. [CrossRef]
86. Sun, W.B.; Li, H. Research progress on zircon from pegmatites and insights into rare-metal mineralization—A review. *Earth Sci. Front.* **2023**, *30*, 171–184. (In Chinese with English abstract)
87. Fabricio-Silva, W.; Rosière, C.A.; Bühn, B. The shear zone-related gold mineralization at the Turmalina deposit, Quadrilátero Ferrífero, Brazil: Structural evolution and the two stages of mineralization. *Miner. Depos.* **2019**, *54*, 347–368. [CrossRef]
88. Wang, T.; Tong, Y.; Jahn, B.; Zou, T.R.; Wang, Y.B.; Hong, D.W.; Han, B.F. SHRIMP U–Pb Zircon geochronology of the Altai No. 3 Pegmatite, NW China, and its implications for the origin and tectonic setting of the pegmatite. *Ore Geol. Rev.* **2007**, *32*, 325–336. [CrossRef]
89. Wang, C.; Liu, L.; Yang, W.Q.; Zhu, X.H.; Cao, Y.T.; Kang, L.; Chen, S.F.; Li, R.S.; He, S.P. Provenance and ages of the Altyn Complex in Altyn Tagh: Implications for the early Neoproterozoic evolution of northwestern China. *Precambrian Res.* **2013**, *230*, 193–208. [CrossRef]
90. Zhang, K. Geochronology, Geochemistry of Early Paleozoic Igneous Rocks in Tashisayi Area, South Altyn Tagh and Its Geological Signification. Ph.D. Thesis, Northwest University, Xi'an, China, 2018. (In Chinese with English abstract).
91. Cowgill, E.; Yin, A.N.; Harrison, T.M. Reconstruction of the Altyn Tagh fault based on U-Pb geochronology: Role of back thrusts, mantle sutures, and heterogeneous crustal strength in forming the Tibetan Plateau. *J. Geophys. Res. Solid Earth* **2003**, *108*, 7.
92. Qi, X.X.; Li, H.B.; Wu, C.L.; Yang, J.S.; Zhang, J.X.; Meng, F.C.; Shi, R.D.; Chen, S.Y. SHRIMP U-Pb zircon dating for Qiashikansayi granodiorite, the northern Altyn Tagh mountains and its geological implications. *Chin. Sci. Bull.* **2005**, *50*, 440–445. [CrossRef]
93. Hao, J.; Wang, E.Q.; Liu, X.H.; Sang, H.Q. Jinyanshan collisional orogenic belt of the early Paleozoic in the Altun mountains: Evidence from single zircon U-Pb and 40Ar/39Ar isotopic dating for the arc magmatite and ophiolitic mélange. *Acta Petrol. Sin.* **2006**, *22*, 10. (In Chinese with English abstract)
94. Wu, C.L.; Yao, S.Z.; Zeng, L.S.; Yang, J.S.; Wooden, J.L.; Chen, S.Y.; Frank, K.M. Bashikaogong-Shimierbulake granitic complex, north Altun, NW China: Geochemistry and zircon SHRIMP ages. *Sci. China Ser. D Earth Sci.* **2006**, *49*, 1233–1251. [CrossRef]
95. Wu, C.L.; Yang, J.S.; Robinson, P.T.; Wooden, J.L.; Frank, K.M.; Gao, Y.H.; Wu, S.P.; Chen, Q.L. Geochemistry, age and tectonic significance of granitic rocks in north Altun, northwest China. *Lithos* **2009**, *113*, 423–436. [CrossRef]
96. Yang, Z.J. *Early Palaeozoic Tectonic Evolution in HongLiuGou, Altyn, Xinjiang*; Chinese Academy of Geological Science: Beijing, China, 2012; (In Chinese with English abstract).
97. Zhang, Z.W.; Huang, G.; Li, H.M.; Zhang, W.F. LA-ICP-MS zircon U-Pb geochronology and geochemistry of gabbro and diorite from Qilesayi pluton in Lapeiquan area of northern Altun Mountains and their tectonic implications. *Acta Petrol. Mineral.* **2012**, *31*, 13–27. (In Chinese with English abstract)
98. Han, F.B.; Chen, B.L.; Cui, L.L.; Wang, S.X.; Chen, Z.L.; Jiang, R.B.; Li, L.; Qi, W.X. Zircon SHRIMP U-Pb age of intermediate-acid intrusive rocks in Kaladawan area, eastern Altun Mountains, NW China, and its implications. *Acta Petrol. Sin.* **2012**, *28*, 2277–2291. (In Chinese with English abstract)
99. Wu, D.; Zheng, K.; Wu, C.L.; Chen, H.J.; Gao, D.; Zou, F.H. Geochronology and geochemistry of the Bashikaogong S-type granitic rocks: A record of Early Paleozoic subduction and collision in North Altun, Northwestern China. *Arab. J. Geosci.* **2021**, *14*, 1327. [CrossRef]
100. Meng, L.T.; Chen, B.L.; Zhao, N.N.; Wu, Y.; Zhang, W.G.; He, J.T.; Wang, B.; Han, M.M. The distribution, geochronology and geochemistry of early Paleozoic granitoid plutons in the North Altun orogenic belt, NW China: Implications for the petrogenesis and tectonic evolution. *Lithos* **2017**, *268*, 399–417. [CrossRef]

101. Yu, S.Y.; Zhang, J.X.; Li, S.Z.; Sun, D.Y.; Peng, Y.B.; Zhao, X.L. Continuity of the North Qilian and North Altun orogenic belts of NW China: Evidence from newly discovered Palaeozoic low-Mg and high-Mg adakitic rocks. *Geol. Mag.* **2018**, *155*, 1684–1704. [CrossRef]
102. Xinjiang Bureau of Geology and Mineral Resources Exploration and Development. 1:250,000 Geological Map of the Suwushijie Area. 2003; 1–275, unpublished. (In Chinese)
103. Kang, L. Early Paleozoic Multi-Stage Granitic Magmatism and the Geological Significance in the South Altyn Tagh HP-UHP Metamorphic Belt. Ph.D. Thesis, Northwest University, Xi'an, China, 2014. (In Chinese with English abstract).
104. Zhang, R.Y.; Zeng, Z.C.; Zhu, W.P.; Chen, N.; Zhao, J.L.; Li, Q.; Wang, Q.W.; Rao, J.W. LA-ICP-MS zircon U-Pb dating, geochemical features and their geological implications of Paxialayidang plutons on the southern margin of Altyn Tagh. *Geol. Rev.* **2016**, *62*, 1283–1299. (In Chinese with English abstract)
105. Huang, Y.Q.; Wu, M.Q.; Germain, B.; Yu, H.C.; Qiao, B.X.; Zhao, Z.G.; Qiu, K.F. Geodynamic setting and ore formation of the Younusisayi thorium deposit in the Altyn orogenic belt, NW China. *Ore Geol. Rev.* **2022**, *140*, 104552. [CrossRef]
106. Patiño Douce, A.E.; Johnston, A.D. Phase equilibria and melt productivity in the pelitic system: Implications for the origin of peraluminous granitoids and aluminous granulites. *Contrib. Mineral. Pet.* **1991**, *107*, 202–218. [CrossRef]
107. Castro, A.; Patiño Douce, A.E.; Corretgé, L.G.; Rosa, J.D.; El Biad, M.; El-Hmidi, H. Origin of peraluminous granites and granodiorites, Iberian massif, Spain: An experimental test of granite petrogenesis. *Contrib. Mineral. Petrol.* **1999**, *135*, 255–276. [CrossRef]
108. Watson, E.B.; Capobianco, C.J. Phosphorus and the rare earth elements in felsic magmas: An assessment of the role of apatite. *Geochim. Cosmochim. Acta* **1981**, *45*, 2349–2358. [CrossRef]
109. Wolf, M.B.; London, D. Apatite dissolution into peraluminous haplogranitic melts: An experimental study of solubilities and mechanisms. *Geochim. Cosmochim. Acta* **1994**, *58*, 4127–4145. [CrossRef]
110. Li, X.H.; Li, W.X.; Li, Z.X. On the genetic classification and tectonic implication of the Early Yanshanian granitoids in the Nanling rang. South China. *Chin. Sci. Bull.* **2007**, *52*, 981–992. (In Chinese with English abstract)
111. Chappell, B.W.; White, A.J.R. I-and S-type granites in the Lachlan Fold Belt. *Earth Environ. Sci. Trans. R. Soc. Edinb.* **1992**, *83*, 1–26.
112. Clemens, J.D. S-type granitic magmas-petrogenetic issues, models and evidence. *Earth-Sci. Rev.* **2003**, *61*, 1–18. [CrossRef]
113. Maniar, P.D.; Piccoli, P.M. Tectonic discrimination of granitoids. *Geol. Soc. Am. Bull.* **1989**, *101*, 635–643. [CrossRef]
114. Peccerillo, A.; Taylor, S.R. Geochemistry of Eocene Calc-alkaline volcanic rocks from the Kastamonu Area, Northern Turkey. *Contrib. Mineral. Petrol.* **1976**, *56*, 63–81. [CrossRef]
115. Jahns, R.H.; Burnham, C.W. Experimental studies of pegmatite genesis; I, A model for the derivation and crystallization of granitic pegmatites. *Econ. Geol.* **1969**, *64*, 843–864. [CrossRef]
116. Shearer, C.K.; Papike, J.J.; Redden, J.A.; Simon, S.B.; Walker, R.J.; Laul, J.C. Origin of pegmatitic granite segregations, Willow Creek, Black Hills, South Dakota. *Can. Mineral.* **1987**, *25*, 159–171.
117. London, D. Internal differentiation of rare-element pegmatites: A synthesis of recent research. *Geol. Soc. Am. Spec. Pap.* **1990**, *246*, 35–50.
118. Webster, J.D.; Thomas, R.; Rhede, D.; Förster, H.J.; Seltmann, R. Melt inclusions in quartz from an evolved peraluminous pegmatite: Geochemical evidence for strong tin enrichment in fluorine-rich and phosphorus-rich residual liquids. *Geochim. Cosmochim. Acta* **1997**, *61*, 2589–2604. [CrossRef]
119. Simmons, W.B.; Foord, E.E.; Falster, A.U.; King, V.T. Evidence for an anatectic origin of granitic pegmatites, western Maine, USA. *Geol. Soc. Am. Abstr. Programs* **1995**, *27*, A411.
120. Shaw, R.A.; Goodenough, K.M.; Roberts, N.M.W.; Horstwood, M.S.A.; Chenery, S.R.; Gunn, A.G. Petrogenesis of rare-metal pegmatites in high-grade metamorphic terranes: A case study from the Lewisian Gneiss Complex of north-west Scotland. *Precambrian Res.* **2016**, *281*, 338–362. [CrossRef]
121. Müller, A.; Romer, R.L.; Pedersen, R.B. The Sveconorwegian Pegmatite Province—Thousands of pegmatites without parental granites. *Can. Mineral.* **2017**, *55*, 283–315. [CrossRef]
122. Linnen, R.L.; Keppler, H. Melt composition control of Zr/Hf fractionation in magmatic processes. *Geochim. Cosmochim. Acta* **2002**, *66*, 3293–3301. [CrossRef]
123. Zaraisky, G.P.; Aksyuk, A.M.; Devyatova, V.N.; Udoratina, O.V.; Chevychelov, V.Y. Zr/Hf ratio as an indicator of fractionation of rare-metal granites by the example of the Kukulbei complex, eastern Transbaikalia. *Petrology* **2008**, *16*, 7710–7736. [CrossRef]
124. Černý, P.; Meintzer, R.E.; Anderson, A.J. Extreme fractionation in rare-element granitic pegmatites: Selected examples of data and mechanisms. *Can. Mineral.* **1985**, *23*, 381–421.
125. Ballouard, C.; Poujol, M.; Boulvais, P.; Branquet, Y.; Tartèse, R.; Vigneresse, J.L. Nb-Ta fractionation in peraluminous granites: A marker of the magmatic hydrothermal transition. *Geology* **2016**, *44*, 231–234. [CrossRef]
126. Knoll, T.; Huet, B.; Schuster, R.; Mali, H.; Ntaflos, T.; Hauzenberger, C. Lithium pegmatite of anatectic origin-A case study from the Austroalpine Unit Pegmatite Province (Eastern European Alps): Geological data and geochemical model. *Ore Geol. Rev.* **2023**, *154*, 105298. [CrossRef]
127. Dill, H.G. Geology and chemistry of Variscan-type pegmatite systems (SE Germany)–with special reference to structural and chemical pattern recognition of felsic mobile components in the crust. *Ore Geol. Rev.* **2018**, *92*, 205–239.
128. Zhang, H.; Lv, Z.H.; Tang, Y. Metallogeny and prospecting model as well as prospecting direction of pegmatite-type rare metal ore deposits in Altay orogenic belt, Xinjiang. *Miner. Depos.* **2019**, *38*, 792–814. (In Chinese with English abstract)

129. Xu, Z.Q.; Li, S.T.; Zhang, J.X.; Yang, J.S.; He, B.Z.; Li, H.B.; Lin, C.S.; Cai, Z.H. Paleo-Asian and Tethyan tectonic systems with docking the Tarim block. *Acta Petrol. Sin.* **2011**, *27*, 1–22. (In Chinese with English abstract)
130. Şengör, A.M.C.; Natal'In, B.A.; Burtman, V.S. Evolution of the Altaid tectonic collage and Palaeozoic crustal growth in Eurasia. *Nature* **1993**, *364*, 299–307.
131. Pan, G.; Wang, L.; Li, R.; Yuan, S.H.; Ji, W.H.; Yin, F.G.; Zhang, W.P.; Wang, B.D. Tectonic evolution of the Qinghai-Tibet plateau. *J. Asian Earth Sci.* **2012**, *53*, 3–14.
132. Gao, X.F.; Xiao, P.X.; Guo, L.; Dong, Z.C.; Xi, R.G. Opening of an early Paleozoic limited oceanic basin in the northern Altyn area: Constraints from plagiogranites in the Hongliugou-Lapeiquan ophiolitic mélange. *Sci. China Earth Sci.* **2011**, *54*, 1871–1879. (In Chinese with English abstract) [CrossRef]
133. Gai, Y.S.; Liu, L.; Kang, L.; Yang, W.Q.; Liao, X.Y.; Wang, Y.W. The origin and geologic significance of plagiogranite in ophiolite belt at North Altyn Tagh. *Acta Petrol. Sin.* **2015**, *31*, 2549–2565. (In Chinese with English abstract)
134. Zhang, J.X.; Meng, F.C.; Yu, S.Y.; Chen, W.; Chen, S.Y. ^{39}Ar-^{40}Ar geochronology of high-pressure/low-temperature blueschist and eclogite in the North Altyn Tagh and their tectonic implications. *Geol. China* **2007**, *34*, 558–564. (In Chinese with English abstract)
135. Zhang, J.X.; Meng, F.C.; Yu, S.Y. Two contrasting HP/LT and UHP metamorphic belts: Constraint on Early Paleozoic orogeny in Qilian-Altun orogen. *Acta Petrol. Sin.* **2010**, *26*, 1967–1992. (In Chinese with English abstract)
136. Chen, B.L.; Li, S.B.; Jiang, R.B.; Chen, Z.L.; Han, F.B.; Cui, L.L.; Li, L.; Zhao, S.M.; Qi, W.X.; Yang, Y.; et al. Zircon SHRIMP U-Pb dating of intermediate-felsic volcanic rocks from the Kaladawan area, Altun Mountains and its tectonic environment. *Acta Geol. Sin.* **2016**, *90*, 708–727. (In Chinese with English abstract)
137. Meng, L.T.; Chen, B.L.; Luo, D.K.; Wang, Y.; Sun, Y.; Wu, Y.; Zhang, H.; Wang, T. SHRIMP Zircon U-Pb Geochronology of Northern 4337Highland Granodiorite in Kaladawan Area of Northern Altun Mountains and Its Tectonic Implications. *J. Jilin Univ. Earth Sci. Ed.* **2015**, *45*, 1757–1771. (In Chinese with English abstract)
138. Liu, J.H. The Associations, Geochronology and Geochemistry of Igneous Rocks in Lapeiquan, North Altyn Tagh and Its Tectonic Significance. Ph.D. Thesis, Northwest University, Xi'an, China, 2017. (In Chinese with English abstract).
139. Wang, C.M.; Tang, H.S.; Zheng, Y. Early Paleozoic magmatism and metallogeny related to Proto-Tethys subduction: Insights from volcanic rocks in the northeastern Altyn Mountains, NW China. *Gondwana Res.* **2019**, *75*, 134–153. [CrossRef]
140. Zheng, K.; Wu, C.; Lei, M.; Zhang, X.; Chen, H.J.; Wu, D.; Gao, D. Petrogenesis and tectonic implications of granitoids from western North Altun, Northwest China. *Lithos* **2019**, *340*, 255–269. [CrossRef]
141. Ye, X.T.; Zhang, C.L.; Wang, Q.; Wang, G.D. Subduction initiation of Proto-Tethys Ocean and back-arc extension in the northern Altun Mountains, northwestern China: Evidence from high-Mg diorites and A-type rhyolites. *Lithos* **2020**, *376*, 105748. [CrossRef]
142. Wu, Y.; Chen, Z.L.; Chen, B.L.; Wang, Y.; Sun, Y.; Meng, L.T.; He, J.T.; Wang, B. Early Palaeozoic syn-collisional granitic magmatism in the North Altun and its implication for accretionary orogenic processes. *Acta Petrol. Sin.* **2021**, *37*, 1321–1346. (In Chinese with English abstract)
143. Liu, Q.; Tsunogae, T.; Zhao, G.C.; Li, J.H.; Yao, J.L.; Han, Y.G.; Wang, P. Multiphase ophiolite formation in the Northern Altyn Tagh Orogen, southeastern Tarim. *Am. J. Sci.* **2021**, *321*, 788–821. [CrossRef] [PubMed]
144. Liu, L.; Sun, Y.; Luo, J.H.; Wang, Y.; Chen, D.; Zhang, A.D. Ultra-high pressure metamorphism of granitic gneiss in the Yinggelisayi area, Altun Mountains, NW China. *Sci. China (Ser. D Earth Sci.)* **2004**, *47*, 338–346. [CrossRef]
145. Liu, L.; Zhang, J.; Green, H.W., II; Jin, Z.; Bozhilov, K.N. Evidence of former stishovite in metamorphosed sediments, implying subduction N350 km. *Earth Planet. Sci. Lett.* **2007**, *263*, 180–191. [CrossRef]
146. Wang, C.; Liu, L.; Chen, D.; Cao, Y.T. Petrology, geochemistry, geochronology, and metamorphic evolution of garnet peridotites from South Altyn Tagh UHP terrane, northwestern China: Records related to crustal slab subduction and exhumation history. In *Ultrahigh-Pressure Metamorphism*; Elsevier: Amsterdam, The Netherlands, 2011; pp. 541–577.
147. Cao, Y.T. HP-UHP Metamorphic Evolution and Fluid Activity from the South Altyn Tagh and Shenglikou Area. Ph.D. Thesis, Northwest University, Xi'an, China, 2013. (In Chinese with English abstract).
148. Dong, J.; Wei, C.; Chen, J.; Zhang, J.X. P–T–t path of garnetites in South Altyn Tagh, West China: A complete record of the ultradeep subduction and exhumation of continental crust. *J. Geophys. Res. Solid Earth* **2020**, *125*, e2019JB018881. [CrossRef]
149. Dong, J.; Wei, C. Multi-stage metamorphism of the South Altyn ultrahigh-pressure metamorphic belt, West China: Insights into tectonic evolution from continental subduction to arc–backarc extension. *J. Petrol.* **2021**, *62*, egab082. [CrossRef]
150. Gao, D. Study on the Petrogenesis and Tectonic Geological Significance of the Yusupuleke Tagh Granitic Composite Intrusion, Southern Altun. Ph.D. Thesis, Chang'an University, Xi'an, China, 2017. (In Chinese with English abstract).
151. Kang, L.; Xiao, P.X.; Gao, X.F.; Gao, X.F.; Xi, R.G.; Yang, Z.C. Age, petrogenesis and tectonic implications of Early Devonian bimodal volcanic rocks in the South Altyn, NW China. *J. Asian Earth Sci.* **2015**, *111*, 733–750. [CrossRef]
152. Wu, S.P.; Wu, C.L.; Chen, Q.L. Characteristics and tectonic setting of the Tula aluminous A- type gr anite at the south side of the Altyn Tagh fault, NW China. *Geol. Bull. China* **2007**, *26*, 1385–1392. (In Chinese with English abstract)
153. Wang, C.; Liu, L.; Zhang, A.D.; Yang, W.Q.; Cao, Y.T. Geochemistry and petrography of Early Paleozoic Yusupuleke Tagh rapakivi-textured granite complex, South Altyn: An example for magma mixing. *Acta Petrol. Sin.* **2008**, *24*, 2809–2819. (In Chinese with English abstract)

154. Wang, C.; Liu, L.; Xiao, P.X.; Cao, Y.T.; Yu, H.Y.; Meert, J.G.; Liang, W.T. Geochemical and geochronologic constraints for Paleozoic magmatism related to the orogenic collapse in the Qimantagh–South Altyn region, northwestern China. *Lithos* **2014**, *202*, 1–20. [CrossRef]
155. Zhang, J.X.; Yu, S.Y.; Mattinson, C.G. Early Paleozoic polyphase metamorphism in northern Tibet, China. *Gondwana Res.* **2017**, *41*, 267–289. [CrossRef]

Disclaimer/Publisher's Note: The statements, opinions and data contained in all publications are solely those of the individual author(s) and contributor(s) and not of MDPI and/or the editor(s). MDPI and/or the editor(s) disclaim responsibility for any injury to people or property resulting from any ideas, methods, instructions or products referred to in the content.